



Improving Geothermal Steam Purity for a Wellhead Geothermal Power Plant

Lárus Guðmundsson

Thesis of 60 ECTS credits
**Master of Science in Energy Engineering -
Iceland School of Energy**

December 2014



Improving Geothermal Steam Purity for a Wellhead Geothermal Power Plant

Lárus Guðmundsson

Thesis of 60 ECTS credits submitted to the School of Science and Engineering
at Reykjavík University in partial fulfillment of
the requirements for the degree of
Master of Science in Energy Engineering - Iceland School of Energy

December 2014

Supervisor:

Dr. Einar Jón Ásbjörnsson, Supervisor
Assistant Professor, Reykjavik University

Examiner:

Jónas Matthíasson, Examiner
Vélaverkfræðingur, Verkís verkfræðistofa

Copyright
Lárus Guðmundsson
December 2014

Improving Geothermal Steam Purity for a Wellhead Geothermal Power Plant

Lárus Guðmundsson

60 ECTS thesis submitted to the School of Science and Engineering
at Reykjavík University in partial fulfillment
of the requirements for the degree of
Master of Science in Energy Engineering - Iceland School of Energy.

December 2014

Student:

Lárus Guðmundsson

Supervisor:

Dr. Einar Jón Ásbjörnsson

Examiner:

Jónas Matthíasson

The undersigned hereby grants permission to the Reykjavík University Library to reproduce single copies of this project report entitled **Improving Geothermal Steam Purity for a Wellhead Geothermal Power Plant** and to lend or sell such copies for private, scholarly or scientific research purposes only.

The author reserves all other publication and other rights in association with the copyright in the project report, and except as herein before provided, neither the project report nor any substantial portion thereof may be printed or otherwise reproduced in any material form whatsoever without the author's prior written permission.

Date

Lárus Guðmundsson
Master of Science

Improving Geothermal Steam Purity for a Wellhead Geothermal Power Plant

Lárus Guðmundsson

December 2014

Abstract

For geothermal turbines the purity of the steam can make or break the power plant, high maintenance results in more downtime and less revenue for the power company. In this paper it is attempted to design and model a device that can clean the steam to reduce scaling potential and reduce the maintenance on the turbine by condensing the hot steam partially and by introducing it to intense vorticity to mix the condensed droplets thus reducing the concentration of total dissolved solids (TDS) that are carried over in the brine from the two-phase separator. By introducing the proposed equipment as an addition to the hotter side of the power plant a dilution of TDS in the droplets can be ten-folds in theory, depending on the performance of the mist eliminator that takes out that last condensate.

Úrbætur á gufuhreinleika fyrir holutoppsvirkjanir

Lárus Guðmundsson

Desember 2014

Útdráttur

Í túrbínnum í jarðorkuverum skiptir hreinleiki gufunar mjög miklu máli og getur það verið úrslitavaldur í rekstri orkuversins, mjög hár viðhaldskostnaður og tími þar sem ekki er framleitt rafmagn þýðir minni tekjur fyrir orkufyrirtækið. Í þessari ritgerð verður reynt að hanna módel af kerfi þar sem gufan er hreinsuð til að reyna að draga úr frekari myndun á útfellingum og viðhaldskostnaði á túrbínu samhliða, það er framkvæmt þannig að hluti af heitri gufu er þétt niður um ákveðið magn og hún svo send í gegnum óreiðukennt ástand til að fá góða blöndun á þeim dropum sem stækkað hafa vegna þéttingarinnar með því er hægt að minnka leysni í gufu dropum sem innihalda uppleyst efni (TDS) sem berast frá aðalskilju. Með því að bæta þessum búnaði á heita hluta orkuversins er fræðilega hægt að tífalda leysnina í þéttivatninu sem berst frá rakaskilju miðað hversu vel rakaskiljan skilur þéttivatnið frá gufunni.

Acknowledgements

I would like to extend my sincerest gratitude to everyone who helped and supported me throughout this work. Special thanks to my supervisor Dr. Einar Jón Ásbjörnsson who has encouraged me and helped me through this work, all of my professors at Reykjavik University for their excellent teaching and guidance for if it weren't for them I would not be writing this paper. My sincerest thanks to Green Energy Group and their staff for assisting me and providing me with access to their vast experience and facilities.

Last but not least I would like to thank my fiancé Fanney Hólmfríður Kristjánsdóttir for her endless patience and support during this work. Special thanks to my family and friends who have been there for me during my studies.

Contents

Table of Contents	vii
List of Figures	ix
List of Tables	xi
Nomenclature	xiii
1 Introduction	1
2 Literature review	3
2.1 Wellhead conditions	3
2.1.1 Geothermal fluid	3
2.1.2 Steam purity	4
2.2 Steam properties	5
2.2.1 Steam Quality	5
2.2.2 Steam Separation	6
2.2.3 Steam Gathering System	7
2.3 Condensing steam in a pipeline	9
2.4 Heat exchangers	10
2.4.1 Extended surfaces	13
2.5 Demisters	14
3 Methods	17
3.1 Geometry approach	18
3.1.1 Serrated helical fins	18
3.1.2 Solid helical fins	19
3.2 Heat transfer approach	20
3.2.1 Internal heat transfer correlations	20
3.2.2 External heat transfer correlations	21

3.3	Pressure drop correlation	24
3.3.1	Serrated tube banks	24
3.3.2	Solid tube banks	25
3.4	Concentration of TDS in the carryover	25
3.5	Computational Fluid Dynamics	27
3.5.1	K- ϵ Turbulence Model	27
3.5.2	SST K- ω Turbulence Model	28
3.6	Reaction forces due to thermal expansion	29
3.7	Uncertainty propagation	30
4	Results	33
4.1	Analytical model	33
4.1.1	Design scenarios	35
4.2	CFD model	39
4.3	Reaction forces	44
4.4	Uncertainty propagation results	47
5	Conclusions	49
	References	53
A	Scenario A	57
B	Scenario B	61
C	Other designs	65
C.0.1	Design 1	65
C.0.2	Design 3	66
C.0.3	Design 4	67

List of Figures

1	Wellhead geothermal power plant	1
2	Proposed idea for the process	2
3	Temperature-entropy diagram for water [1] [2]	5
4	T-s diagram showing the separation process [3]	6
5	Types of steam-liquid separators.	7
6	Variations in the steam gathering system as depicted by DiPippo [4].	8
7	The three modes of heat transfer [5]	10
8	Various types of configuration for heat exchangers [6]	11
9	An example of the two most common variations of ACHE with horizontal tube banks. [7]	12
10	Some typical examples of extended surfaces	13
11	Solid and serrated helical finned tubing [8]	13
12	Type of droplet removals within the demister	14
13	Various types of demisters	15
14	Steam droplet from the separator being condensed via the ACHE and through the mist eliminator	25
15	Free body diagrams of the reaction forces due to thermal expansion.	29
16	EES Model interface for the base variables	35
17	Thermal transfer & fan work as a function of face velocity	36
18	Steam quality for serrated and solid fins as a function of face velocity	36
19	Fluid geometry of the different models	40
20	Design 2 without the fluid domain	40
21	Enhancement layering to capture the effects in the boundary layer regime [9]	41
22	Resultant boundary layer effect from Design 2 near the wall.	42
23	Comparison of $k-\epsilon$ and SST $k-\omega$ on Design 2	43
24	Trace particle flow for SST $k-\omega$ in Design 2	43

25	Magnitude of the reaction forces that are acting upon flange at the inlet. . .	45
26	Von Mises stresses for the unit.	45
27	Displacement magnitude exaggerated by 2% of the model size	46
28	Thermal transfer for serrated and solid fins as a function of fin height . . .	57
29	Thermal transfer for serrated and solid fins as a function of fin thickness .	58
30	Thermal transfer for serrated and solid fins as a function of fins per meter	58
31	Thermal transfer for serrated and solid fins as a function of fin spacing . .	59
32	Thermal transfer for serrated and solid fins as a function of fouling factors	59
33	Thermal transfer for serrated and solid fins as a function of fin height . . .	61
34	Thermal transfer for serrated and solid fins as a function of fin thickness .	62
35	Thermal transfer for serrated and solid fins as a function of fins per meter	62
36	Thermal transfer for serrated and solid fins as a function of fin spacing . .	63
37	Thermal transfer for serrated and solid fins as a function of fouling factors	63
38	Topview of $k-\epsilon$ and SST $k-\omega$ on Design 1	65
39	Sideview of $k-\epsilon$ and SST $k-\omega$ on Design 1	66
40	Topview of $k-\epsilon$ and SST $k-\omega$ on Design 3	66
41	Sideview of $k-\epsilon$ and SST $k-\omega$ on Design 3	67
42	Topview of $k-\epsilon$ and SST $k-\omega$ on Design 4	67
43	Sideview of $k-\epsilon$ and SST $k-\omega$ on Design 4	68

List of Tables

1	Steam purity criteria for a geothermal turbine	4
2	ACHE initial conditions and assumptions	34
3	Ranges for the changing ACHE variables and the fixed base variables . .	35
4	Design scenarios	37
5	Results from Scenario A	37
6	Results from Scenario B	39
7	CFD model details and pressure drop results	41
8	Material properties for P235-T1	44
9	Reaction forces (Magnitude)	44
10	Uncertainty propagation for thermal transfer in Scenario A	47
11	Uncertainty propagation for thermal transfer in Scenario B	47

Nomenclature

Abbreviations

ACHE Air Cooled Heat Exchanger

CFD Computational Fluid Dynamics

HTC Heat Transfer Coefficient

LMTD Log Mean Temperature Difference [K]

NCG Non-condensable gases [%]

T-s Temperature-Entropy

TDS Total Dissolved Solids [mg/kg]

TEMA Tubular Exchanger Manufacturers Association

Greek letters

δ Wall roughness [m]

ϵ Specific dissipation rate for the k- ϵ model [J/kg-s]

η_{fan} Fan efficiency [-]

η_{motor} Motor efficiency [-]

γ_p Evaporation fraction from pressure loss [-]

γ_{th} Condensate fraction from thermal losses [-]

μ Kinematic viscosity [kg/m³]

μ_b Bulk kinematic viscosity of air [m²/s]

μ_s Kinematic viscosity of steam [m²/s]

μ_t Kinematic Eddy viscosity [m²/s]

ν_t	Kinematic Eddy Viscosity for the SST k- ω model	[m ² /s]
ω	Specific dissipation rate for the SST k- ω model	[J/kg-s]
ρ	Density	[kg/m ³]
ρ_1	Density of air entering the ACHE	[kg/m ³]
ρ_2	Density of air leaving the ACHE	[kg/m ³]
ρ_b	Bulk density of air	[kg/m ³]
ρ_s	Steam density	[kg/m ³]

Variables

ΔP	Differential pressure across	[Pa]
\dot{m}_s	Steam mass flow rate	[kg/s]
\dot{m}_{air}	Mass flow of air	[kg/s]
C_1	Correction factor for they Reynolds number	[-]
C_2	Correction factor for they Reynolds number	[-]
C_3	Correction factor for the geometry of the fins	[-]
C_4	Correction factor for the geometry of the fins	[-]
C_5	Correction factor for the spacing between rows and tubes	[-]
C_6	Correction factor for the spacing between rows and tubes	[-]
E	Fin efficiency factor	[-]
Nu_s	Nusselt number steam side	[-]
Pr_s	Prandtl number steam side	[-]
Re_s	Reynolds number steam side	[-]
Re_{air}	Reynolds number for the air side	[-]
A	Surface area	[m ²]
a	Flow acceleration factor	[-]
A_c	Cross sectional area of the tube bank	[m ²]
A_i	Internal surface area on the steam side	[m ²]
A_n	Net free area in a row	[m ²]

$A_{o,serr}$	External surface area for a serrated fin type on the air side	[m ²]
$A_{o,solid}$	External surface area of solid helical type fins	[m ²]
A_{po}	Prime outside surface area	[m ²]
$c_{p,air}$	Specific heat of air	[J/kg-K]
$c_{p,s}$	Specific heat of steam	[J/kg-K]
D_f	Outside diameter of finned tube	[m]
D_i	Inside diameter	[m]
D_o	Outer diameter of the tube	[m]
E_{ij}	Component of the deformation rate (Strain rate)	[1/s]
f	Friction factor	[-]
F_1	First blending function	[-]
F_2	Second blending function	[-]
f_s	Fin spacing between fins transversely	[m]
G_n	Air mass flux	[kg/s-m ²]
g_x	Gravitational force in the x-direction	[m/s ²]
g_y	Gravitational force in the y-direction	[m/s ²]
g_z	Gravitational force in the z-direction	[m/s ²]
h_c	Averaged air side heat transfer coefficient	[W/m ² -K]
h_e	Effective air side heat transfer coefficient	[W/m ² -K]
h_i	Internal heat transfer coefficient steam side	[W/m ² -K]
h_o	Averaged air side heat transfer coefficient with outside fouling	[W/m ² -K]
h_{fg}	Latent heat	[kJ/kg]
h_f	Saturated liquid enthalpy	[kJ/kg]
h_{gp}	Saturated vapour enthalpy after ACHE	[kJ/kg]
h_g	Saturated vapour enthalpy	[kJ/kg]
h_{in}	Enthalpy entering the heat exchanger	[J/kg]
h_{out}	Enthalpy leaving the heat exchanger	[J/kg]

j	Colburn heat transfer factor	[-]
k	Turbulent Kinetic Energy	[J/kg]
k_b	Bulk thermal conductivity of air	[W/m-K]
k_f	Fin thermal conductivity	[W/m-K]
k_s	Thermal heat conductivity of the steam	[W/m-K]
L	Length of the tube bundle	[m]
l_f	Height of fins	[m]
M	Moment of force	[Nm]
N	Total number of tubes	[-]
n_f	Number of fins per meter	[fins/m]
N_r	Number of tube rows	[-]
N_t	Number of tubes per row	[-]
P_k	Production limiter	[-]
P_l	Longitudinal tube pitch	[m]
P_t	Transverse tube pitch	[m]
Q	Thermal heat transfer rate	[W]
R_1	Reaction forces at location 1	[N]
R_2	Reaction forces at location 2	[N]
R_{fi}	Steam side fouling factor	[m ² -K/W]
R_{fo}	Air side fouling factor	[m ² -K/W]
s_f	Spacing between fins	[m]
t	Time	[seconds]
T_b	Bulk outside temperature	[K]
t_f	Thickness of each fin	[m]
T_s	Average fin temperature	[K]
T_∞	Ambient air temperature	[K]
T_{out}	Temperature of air leaving	[K]

T_{sat}	Saturation temperature of the steam	[K]
U	Over all heat transfer coefficient	[W/m ² -K]
u	Velocity component in the x-direction	[m/s]
U_o	Over-all heat transfer coefficient based on the outside surface area	[W/m ² -K]
v	Velocity component in the y-direction	[m/s]
v_s	Average steam velocity	[m/s]
V_{fan}	Velocity going through the fan	[m/s]
W	Width of the tube bundle	[m]
w	Velocity component in the z-direction	[m/s]
w_s	Width of segmented fin	[m]
W_{fan}	Power the fan requires	[W]
W_{motor}	Power the motor requires	[W]
x	Depicts the x-axis in the Cartsian coordinate system	[-]
x_i	Directional component in the i or j direction	[-]
y	Depicts the y-axis in the Cartsian coordinate system	[-]
z	Depicts the z-axis in the Cartsian coordinate system	[-]

Chapter 1

Introduction

Wellhead geothermal power plants are becoming popular in the industry since they utilize only one well at a time, thus minimizing the cost of constructing large power plants and steam transmission lines, the steam can be harnessed right away from the wellhead and it can be optimized for each individual well. By constructing one modular power plant for each well, lead times are significantly reduced and within a year power can be harnessed from the well. The traditional power plants gather steam and are limited to a 2-5 km radius from the well, with the wellhead geothermal power plant there is no limit since the only lines connected to the power plant will be the electric transmission lines [10].

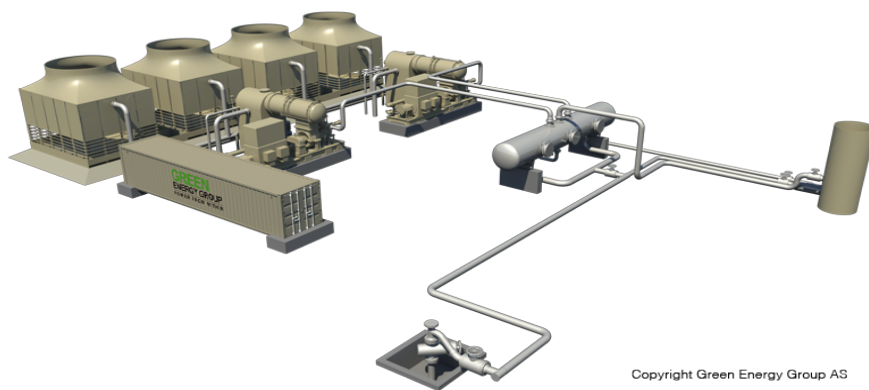


Figure 1: Wellhead geothermal power plant

The governing factor in a successful geothermal power plant is determining the well conditions, what the concentration of contaminants are within the well such that precautions can be made to prevent any types of scaling, corrosion and erosion. Once the well conditions have been determined to a degree of certainty it is possible to start to model the power plant from the given conditions.

Important factor in producing power from a steam turbine is the steam quality and purity that the turbine is subjected to, by cleaning the steam prior to it entering the turbine you can ensure less down time and a longer operational lifetime of the turbine [11]. To clean the steam there are various methods that can be applied such as scrubbing, condensing and chemical treatments of the steam that can help reducing contaminants and droplet sizes. Conventional ways in Iceland have been to condense the steam partially in a long pipeline, 400-1000 meters [12], leading to a demister which removes the larger droplets, then the steam is led from the demister to the turbine resulting in $> 99,99\%$ steam quality which is often the quality a steam turbine manufacturer requires.

The steam quality depends mostly on the steam coming from the separator station, the separator is the key to producing high quality steam in a geothermal power plant. Multiple types of separators are around but they can be classified into two main categories, a horizontal and a vertical separator.

Green Energy Group AS is a company that specializes in modular wellhead geothermal power plants, such as the one on Figure (1), in the range of 3,2 to 6,4 MW per unit [10]. Their solution involves shorter lead time to produce electricity and optimizing each well to its specific needs thus optimizing the electricity generation. To be able to produce power efficiently with reliability you need to have clean and pure steam entering the turbine and to do so multiple scenarios will be looked at to clean and further purify and improve the quality of the steam.

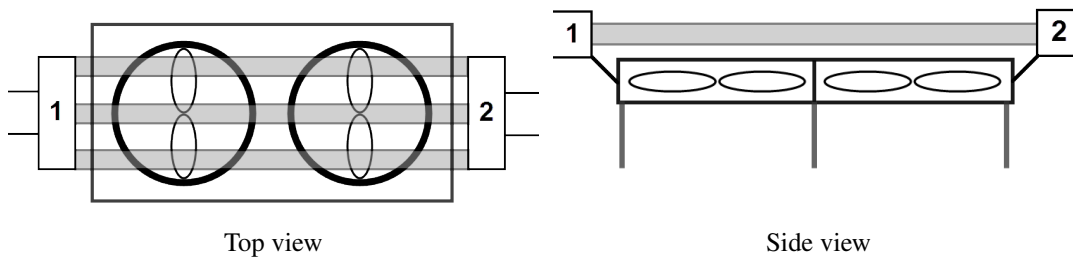


Figure 2: Proposed idea for the process, (1) steam from the separator and (2) where the steam has been condensed slightly.

One idea that will be looked at is to condense the steam partially via forced air convection over tube bundles as is depicted in Figure (2). By using forced air convection, i.e. by using fan(s), the process can be controlled to a greater extent since it is highly dependant upon outside air conditions. The system will be modelled taking into account varying outside temperature and conditions. CFD (Computational Fluid Dynamics) analysis for the fluid behavior and static stresses will be determined to aid in the design.

Chapter 2

Literature review

2.1 Wellhead conditions

Conditions of the well is of great importance, depending on what comes out of the well governs the power plant in a way, depending on pressure and fluid composition. The wellhead power plant needs to adjust to the conditions of each well accordingly. Good example of this is the Reykjanes power plant where the pressure cannot go below a specific limit since the TDS is very high, amorphous silica will precipitate if the pressure is lowered below that limit the precipitated material will adhere to everything in the surface equipment of the plant and cause a shutdown if not handled correctly. [13]

2.1.1 Geothermal fluid

The fluid coming from a geothermal well can be of three principal types [14]:

- Liquid-phase low-temperature which are liquid dominated wells and can have pressure above atmospheric.
- Two-phase high-temperature wells are wells that produce a two-phased fluid in either liquid or vapour phase.
- Dry-steam high-temperature wells where the well is steam-dominated.

Most production wells are of the two-phase kind but there exist fields that are steam dominated, such as the Geysers in California and at Reykjanes where the water level has dropped and boiling is occurring in the reservoir causing a steam cap to be formed in the upper part of the reservoir [15].

Wellhead geothermal power plants work with the two-phased fluid type and separate the fluid to steam and liquid (brine), the steam is then used to power the turbine and the brine is reinjected back to the reservoir through reinjection wells or released out via silencer.

2.1.2 Steam purity

Steam purity covers the contaminants that are carried with the steam, there two basic types of contaminants in the geothermal steam; liquid entrainment and volatile chemical species. Liquid entrainment is commonly resolved by the use of separators and demisters. The volatile species can be distinguished into two groups, the slightly volatile and the highly volatile species. Slightly volatiles such as silica, arsenic and boron and the highly volatiles such as carbon dioxide, hydrogen sulfide and ammonia. [11]

Table 1: Steam purity criteria for a geothermal turbine

Impurities	Scenario 1	Scenario 2	Scenario 3
TDS	<0,5	0,5 - 5	>5
SiO ₂	<0,1	0,1 - 1	>1
Cl	<0,1	0,1 - 1	>1
Fe	<0,1	0,1 - 1	>1

Source: Mitsubishi Operational Manual [16]
All values are in ppm (mg/kg)

The Scenario modes introduced in Table 1 are the following:

- Scenario 1: Continuous normal operation with minimum maintenance.
- Scenario 2: Abnormal operation, requires regular maintenance.
- Scenario 3: The turbine should not be operated.

The numbers in Table 1 are not absolute criteria but should be a guide to turbine operation. An example of another criteria is that allowable operation range is with 0,1 ppm concentration of silica and 15 ppm of TDS, which is not ideal but allowable and should not require maintenance until 2 years of operation (around 10% power loss after 2 years) and the upper limit is 1,0 ppm silica and 50 ppm TDS which would result in roughly 20% power loss in 1 year, requiring vast maintenance [11].

2.2 Steam properties

The properties of water are extensive, the typical diagram given when looking at working cycles is the Temperature-Entropy (T-s) diagram which can show the energy transfer in the system i.e. the area on the T-s diagram is the heat transfer to or from the system. The phase quality of the water can also be determined whether it be in liquid or steam phase.

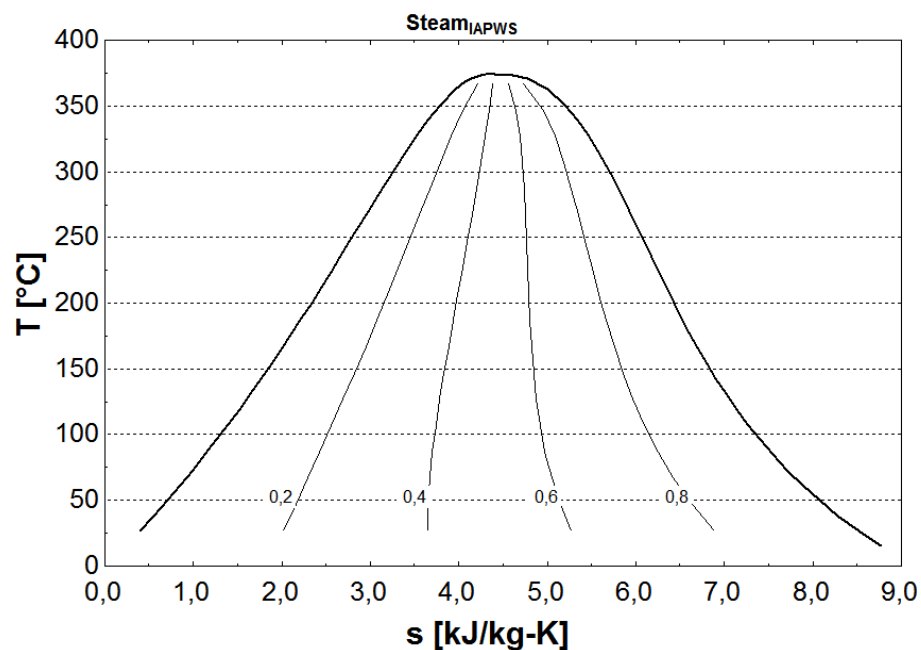


Figure 3: Temperature-entropy diagram for water [1] [2]

When the state is within the bell-curve, shown in Figure 3, the temperature indicates the saturation temperature and depending on how close or far away the specific state is from the curved lines, on either side, indicates the vapour to liquid ratio. The closer the state is to the curve on the left hand side the more liquid is present in the mixture, if the state is closer to the curve on the right hand side the more vapour is present.

2.2.1 Steam Quality

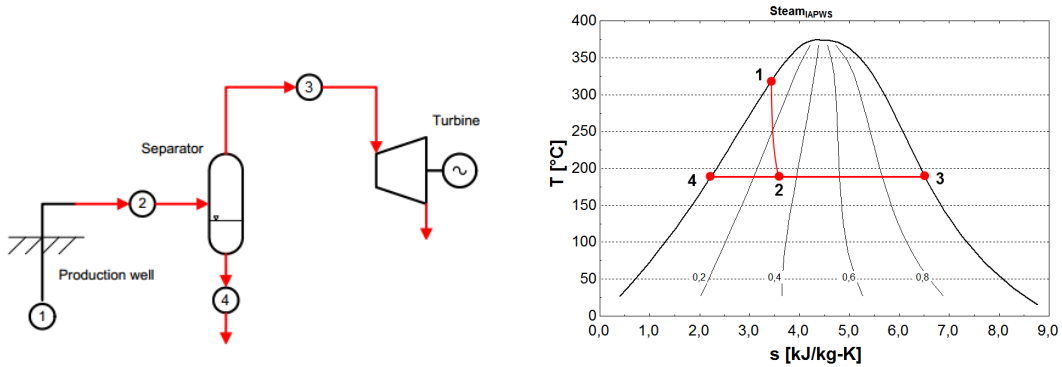
Steam quality is a thermodynamic property of a fluid or a mixture that is saturated. Normally the vapour of the mixture is the fraction, often called dryness fraction, which tells us how much vapour there is currently out of the total mass. Knowing the quality of the fluid is important, it allows us to determine the energy of the saturated fluid.

An example saturation temperature of water at atmospheric conditions is 100°C but the energy content of the water is quite different if it is in the liquid phase or in the vapour

phase, the energy that it takes to go from the liquid phase to the vapour phase is called latent heat or the enthalpy of vaporization and for water at atmospheric conditions it is around 2257 kJ/kg [2].

2.2.2 Steam Separation

The conditions in the well are commonly two-phased conditions and since most of the energy is contained within the steam the two-phased fluid needs to be separated into steam and liquid. The steam is used for electricity generation and the liquid can either be reinjected to the reservoir or to be used further such as double flashing or district heating. The



(1) is the two-phased fluid in the well, (2) is where the pressure has been dropped for the two-phased mixture, (3) shows the steam after separation leading to the turbine and (4) is the separated liquid.

T-s diagram showing an example of a separation process.

Figure 4: T-s diagram showing the separation process [3]

pressure is dropped at the separation station denoted by the number 2 in Figure (4) where the liquid is separated through the use of either vertical or horizontal separators. Commonly horizontal separators (sometimes called gravity separators) are used in Iceland but in other places such as New Zealand the vertical separators are preferred [17].

Horizontal type separators use gravity to separate the two-phased fluid where the fluid enters the chamber the liquid droplets will settle in the tank due to gravity forces and the steam is extracted at an outlet located on top of the chamber at the other end of the vessel from the inlet. On the inlet are usually flow distributors such as baffle plates, diffusers etc. Before the outlet commonly there are wire meshes or guide vanes (chevrons) to trap any larger liquid droplets.

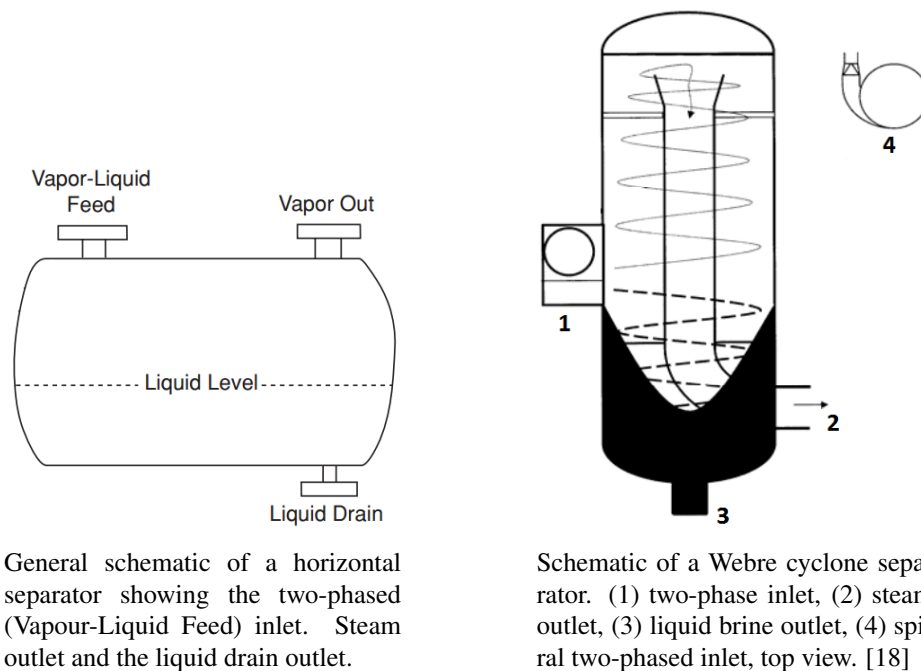


Figure 5: Types of steam-liquid separators.

Vertical separators, they use centrifugal force to separate the liquid from the steam. The heavier larger droplets adhere to the walls of the cylinder due to high momentum and surface tension of the liquid particle.

The separation process is essential to remove as much liquid from the steam as possible, usually the steam quality from the separators are at least 99,9% pure steam [12]. The quality varies between locations and the fluid composition that comes out of the well, the composition of the geothermal fluid is a critical factor for a successful geothermal power plant operation. As mentioned before the steam quality touches upon the ratio of water and steam at the saturation temperature or pressure when it comes to determining the composition of the steam a concept is introduced that is called a steam purity, there is a vast difference between the purity and the quality of a steam, the quality is an indication of the state of the fluid but the purity is how pure the steam is i.e. how much pure water is to other constituents.

2.2.3 Steam Gathering System

Before the wellhead geothermal power plant types, the conventional way to gather steam was to drill multiple wells and gather them in a steam gathering system, which brought the steam to separator station where the steam was separated from the liquid phase of the

two-phased fluid. The steam is then piped to the power house which contains the turbine. Multiple variations exist of the gathering system such as all the wells connect to a single large separator at the power house, a separator at each wellhead, few of wells (2-3 wells) connected to the separator, as is depicted in Figure 6.

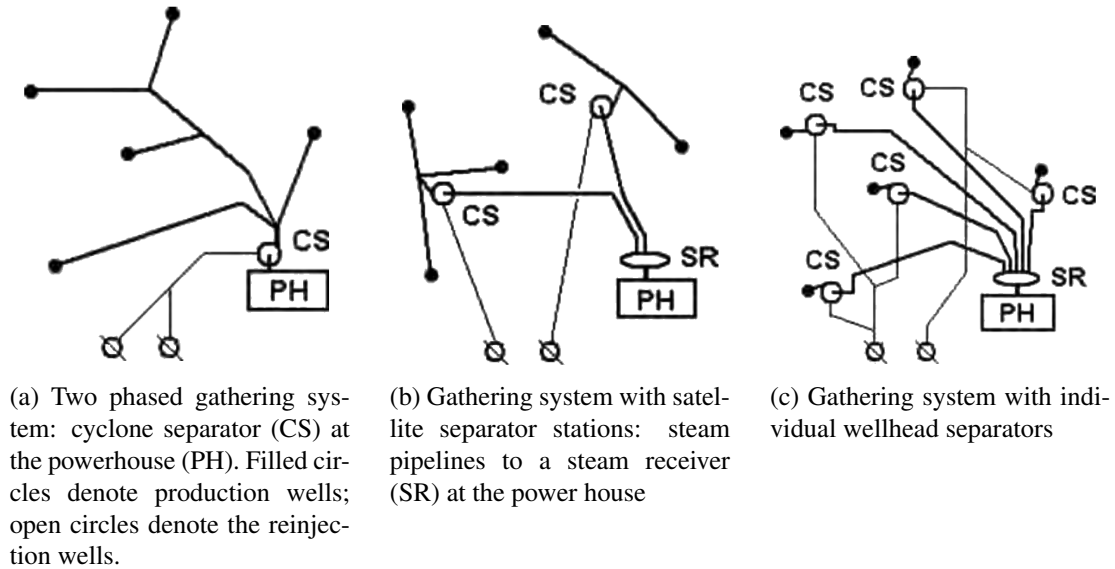


Figure 6: Variations in the steam gathering system as depicted by DiPippo [4].

It is preferred not to have long pipelines containing two-phased fluid since the risk of slug flow is present, thus ideally it is favourable to separate the steam and liquid as soon as possible, however in doing so the number of separators and maintenance cost increases. Slug flow, sometimes referred to as *The Water hammer*, is a two-phased flow regime that can produce slugs of water moving with a large momentum and can have devastating effects on the pipe system such as knocking the pipes off of their concrete foundations and shatter the pipeline.

The benefit of having separator stations at each well is that the pipeline containing the steam has heat and pressure loss relative to the length of the pipeline and materials used. The heat and pressure loss result in the steam condensing in the pipeline, when condensation occurs the tiny water droplets within in the steam grow larger which is not good for the turbine, thus a demister is introduced very close to the inlet of the turbine to remove the larger droplets that are produced by the condensing process in the pipeline.

Since the separators are not able to fully remove the larger droplets this process of condensing the steam in the pipeline and removing the droplets through the demister, which consists of a drum with a knitted mesh and or chevron vanes inside to retrain the larger droplets. The length of the steam pipeline is commonly 400-1000 meters depending on the design of the pipeline and outside conditions [12].

2.3 Condensing steam in a pipeline

When dry saturated steam is travelling through transmission pipelines two things are important to be aware of, pressure drop and heat loss.

As the pressure drops in the pipeline due to frictional forces in the flow such as elevation changes, bends and roughness of the pipe the small droplets within the steam start to boil and get smaller. The pressure drop is accounted for during the design process of the plant such that the inlet pressure for the turbine is not affected by the transmission pressure drop.

Heat loss from the transmission pipeline is equally if not more important as the pressure drop, both of those factors need to be accounted for. The heat loss that occurs due to the temperature difference inside the pipe and outside causes the steam to condense along the pipeline walls and starts to accumulate in the bottom of the pipe, drains for the condensate is located on regular intervals on the pipeline to remove the condensate or the condensate is removed through the demister, it all depends on the layout of the pipe. As the steam moves along the pipeline it generally condenses more than it evaporates since the overall heat loss is more significant than the overall pressure drop and therefore condensate starts to form which is good in the sense of diluting unwanted constituents that are carried over by the steam from the separator, such constituents are Silica, Iron and Chloride (SiO_2 , Fe and Cl respectively) these are unwanted constituents since they can cause depositions of solids on the blades and within the turbine nozzle [19]. NCGs such as hydrogen sulfide can inhibit corrosion if any oxygen is present, carbon dioxide and hydrogen sulfide can cause a severe drop in pH levels of the condensed steam resulting in very acidic condensate within the condenser, the NCG needs to be ejected in the condenser to prevent severe corrosion in the condenser and keeping the condenser at a very low pressure.

In short there are two factors that are at play in the pipeline, pressure drop causes evaporation of the steam condensate and heat loss causes the steam to condense.

2.4 Heat exchangers

The main purpose of heat exchangers is to transfer heat from a hot fluid to a colder fluid, or vice versa depending on application, by three basic methods of heat transfer which are conduction, convection and radiation: [20]

Conduction is heat transfer on the molecular level where atoms interact with each other through lattice vibration between them selves. For a material that does not conduct electricity the main component of the heat transfer is due to vibration. For a conductor the heat transfer occurs mainly through translational motion of free electrons.

Convection is comprised of two mechanisms, random molecular motion (diffusion) and bulk motion of the fluid. As a fluid that is in motion passes a surface at different temperature states heat transfer occurs between the two mediums.

Radiation is where photons are the carrier of the heat energy thus they do not need a medium to transfer thermal energy, the radiation that comes from the sun is a good example of thermal energy being transferred through vacuum by photons. The energy that the photons can carry is governed by the electromagnetic waves generated.

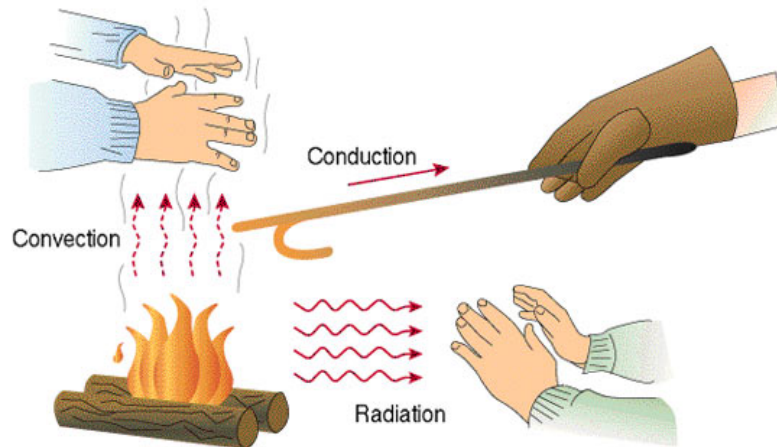


Figure 7: The three modes of heat transfer [5]

For heat exchangers all three modes are encountered but depending on service some can sometimes be neglected such as radiation, but that depends on service. For our sake the radiation effect from the pipes is neglected since the effect is not of great influence to the system as a whole.

As shown in Figure 8 there are many variations of heat exchanger types but most common for air cooled operations are the *X* shell types for cross flow and depending on the number of passes the *A* or *N* front end header, the cover plate is essential for geothermal

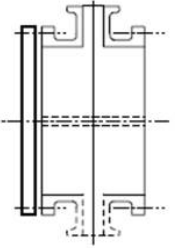
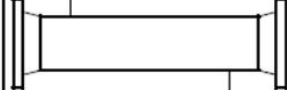
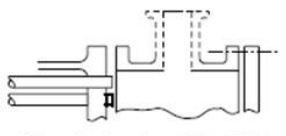
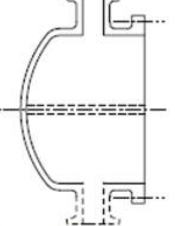
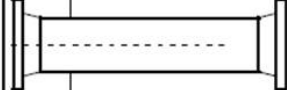
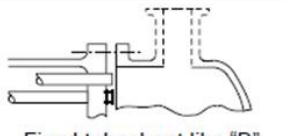
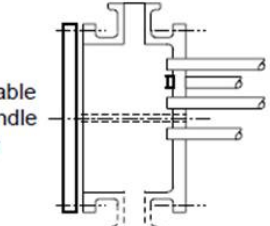
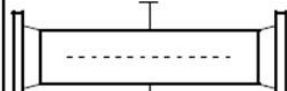
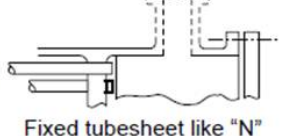
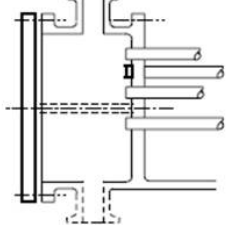
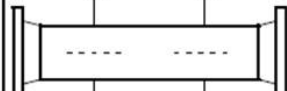
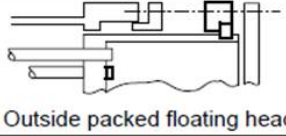

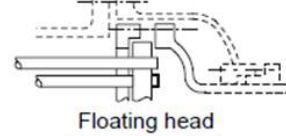
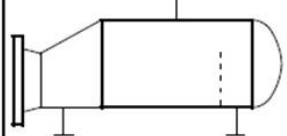
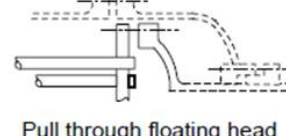
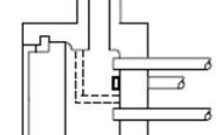
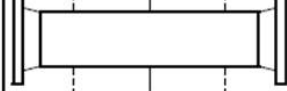
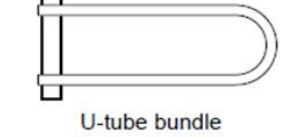
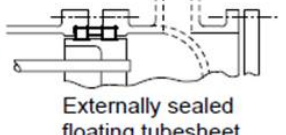
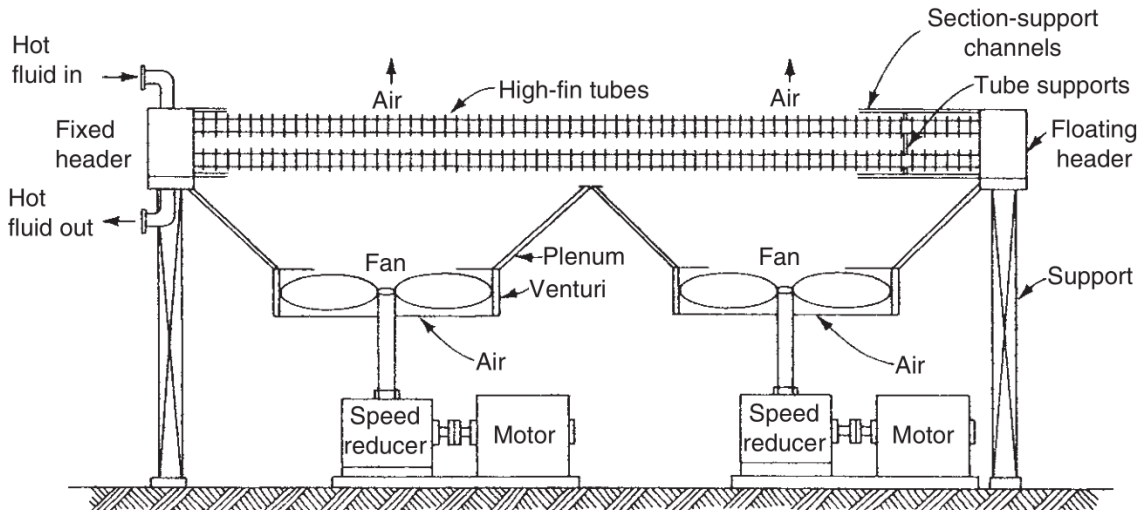
	Front End Stationary Head Types	Shell Types	Rear End Head Types
A	 Channel and removable cover	E  One pass shell	L  Fixed tubesheet like "A" stationary head
B	 Bonnet (integral cover)	F  Two pass shell with longitudinal baffle	M  Fixed tubesheet like "B" stationary head
C	 Removable tube bundle only Channel integral with tubesheet and removable cover	G  Split flow	N  Fixed tubesheet like "N" stationary head
N	 Channel integral with tubesheet and removable cover	H  Double split flow	P  Outside packed floating head
		J  Divided flow	S  Floating head with backing device
		K  Kettle type reboiler	T  Pull through floating head
D	 Special high pressure closure	X  Cross flow	U  U-tube bundle
			W  Externally sealed floating tubesheet

Figure 8: Various types of configuration for heat exchangers [6]

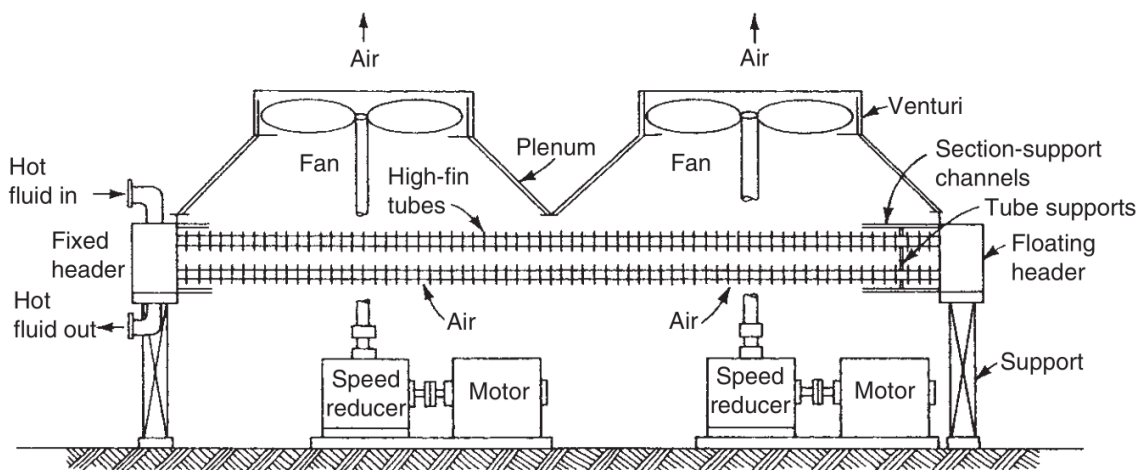
application to be able to conduct maintenance and have the option of viewing the internals to determine scaling, erosion or corrosion.

The design requires us to use a forced draft Air Cooled Heat Exchanger (ACHE), for our case we have chosen to have the N front end header and X shell type, the rear end header is a custom header to achieve mixing, it is a one pass heat exchanger.

There are two types of ACHE, shown in Figure 9 with horizontal tubes the forced and induced draft types. The forced-draft type is often preferred since it is more simpler then the induced-draft. Some of the benefits of using a forced-draft is that there is somewhat



Forced-draft type of an ACHE



Induced-draft type of an ACHE

Figure 9: An example of the two most common variations of ACHE with horizontal tube banks. [7]

less power requirements for the fan due to lower density of the air at the colder side, easier access to maintenance and the fan is not subjected to high temperatures. The advantages of the induced-draft is that the air distribution across the tube bundles is more even, there is less potential for hot air recirculation due to higher exit velocities and less influence from weather conditions such as rain. [7]

2.4.1 Extended surfaces

The effectiveness of a heat exchanger depends on the fluid and the surface area that fluid comes into contact with, the heat is transferred from the hot fluid to the cold fluid and if either of the fluids has low surface area the performance of the heat exchanger will suffer. For mediums such as air the thermal energy the air can carry is very limited since it is essentially a mixture of gas and water vapour and the molecules are not very close to each other so their interaction is limited by the closeness to each other. There for by increasing the surface area the air comes into contact with you are essentially making the air molecules come into contact with the hot or cold surface to be able to carry the thermal energy with it. The industry has experimented with many different

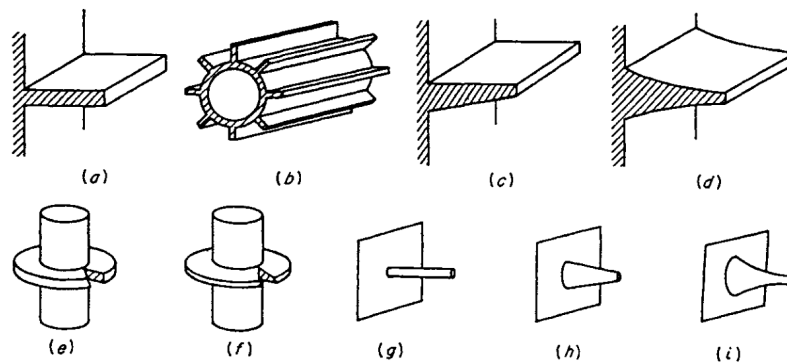


Figure 10: Some typical examples of extended surfaces: (a) longitudinal fin of rectangular profile; (b) cylindrical tube equipped with fins of rectangular profile; (c) longitudinal fin of trapezoidal profile; (d) longitudinal fin of parabolic profile; (e) cylindrical tube equipped with radial fin of rectangular profile; (f) cylindrical tube equipped with radial fin of trapezoidal profile; (g) cylindrical spine; (h) truncated conical spine; (i) truncated parabolic spine. [21]

types of extended surfaces in Figure 10 is a small example of it's variety. The extended surface type covered in this paper is a helical fin with a rectangular profile which has been serrated and an unserrated which from here on will be referred to as serrated and solid helical fins respectively. Figure 11 is an example of these types of fins.



Figure 11: Solid and serrated helical finned tubing [8]

These fins are high frequency welded on to the pipe to minimize the heat affected zone after the weld. Various methods exist to fasten fins to the pipe, various material can be "bonded" together such as aluminium and steel, where grooves are milled into the external pipe wall and aluminium sheet is placed in the groove and then the steel is crumpled around the aluminium sheet to hold it in place. Due to the different metals the thermal expansion is different and by choosing the same material such as carbon steel tubing to carbon steel fins you are minimizing the risk of failing to an extent. For this case we have chosen to use carbon steel for our tubing and fins, it is more cost effective and less likely to mechanical failure.

2.5 Demisters

Demisters remove the last moisture droplets in the steam by using either chevrons (hook-and-vane) and or wire mesh pads. The saturated vapour enters the demister chamber where it gathers and is forced through chevrons, mesh pads or both, which results in removal of the last droplets contained within the saturated steam.



(a) Chevrons



(b) Meshpad

Figure 12: Type of droplet removals within the demister. (Copyright Amistco Separation Products Inc., Alvin, TX)

Chevrons: Chevrons are utilizing a so called *inertial impaction* which is when heavy droplets are travelling through vanes are pushed to the walls due to the momentum of the heavy droplet, some designs incorporate a so called hook where the vanes contain a sort of hooks where they extend outwards from the vanes and capture more droplets. These types are well suited for high velocity steam containing droplets to remove the largest droplets and often the mesh pad comes afterwards to remove the last droplets.

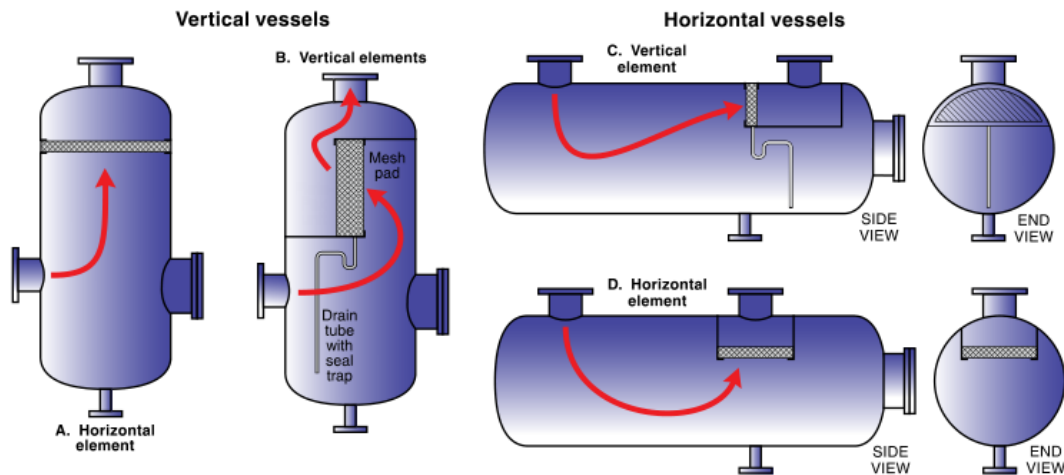


Figure 13: Various types of demisters (Copyright AMACS Process Tower Internals)

Meshpads: Commonly incorporated as the last stage the steam goes through to remove the last droplets, it is a net of wires that capture the droplets as they pass through. These types of pads are not designed to handle as much velocity as the chevrons. Liquid entrainment can be a problem if the steam contains higher amount of liquids than expected then drops will pass through the meshpad and because commonly the velocity profile, depends on fluid entrance, is sort of parabolic in shape (turbulent velocity profile) most commonly entrapment happens at the edges on the meshpad.

Various designs are depicted in Figure 13 and the most common types in Iceland in the geothermal industry are the horizontal demister types, however there are many other design types such as cyclone demisters, each design suites a specific purpose. Common values for the quality of steam exiting demisters is around 99,99% or 99,999%. [22]

Chapter 3

Methods

To begin with it is necessary to follow certain restrictions regarding the condition of the steam within the pipes and the heat exchange process that will take place. First restriction is that the recommended velocities should be around 30-40 m/s and secondly pressure drop within the unit should be kept at minimum.

The conservation of energy needs to be applied and in the case for the ACHE and it consists of three equations:

$$Q = \dot{m}_s \cdot (h_{in} - h_{out}) \quad (1)$$

$$= \dot{m}_{air} \cdot c_{p,air} \cdot (T_{out} - T_{\infty}) \quad (2)$$

$$= U \cdot A \cdot LMTD \quad (3)$$

where Equation (1) represents the energy balance on the steam side, Equation (2) is the air side energy balance and Equation (3) is the ACHE energy balance.

Number of tubes for the heat exchanger are then dependant upon the velocities within them. The mass flow in the main pipe is then related to the cross sectional area of a single tube, velocity within the tube, density of the steam and the number of tubes in the tube bank:

$$\dot{m}_s = \frac{D_i^2 \cdot \pi}{4} \cdot v_s \cdot \rho_s \cdot N \quad (4)$$

The LMTD for fluid at saturation temperature is defined as:

$$LMTD = \frac{T_{out} - T_{\infty}}{\ln \left(\frac{T_{sat} - T_{\infty}}{T_{sat} - T_{out}} \right)} \quad (5)$$

The over all heat transfer coefficient is defined as:

$$\frac{1}{U \cdot A} = \frac{1}{U_o \cdot A_o} = \frac{1}{U_i \cdot A_i} \quad (6)$$

where o and i subscripts denote outside and inside respectively and A denoted by the same subscripts mentioned before represent the surface area.

Determining the outside and inside over all heat transfer coefficient we use empirical correlations that have been evaluated from experimental results.

3.1 Geometry approach

The total width of the bundle is defined as:

$$W = N_t \cdot (D_f + f_s) + 2f_s \quad (7)$$

and the transverse pitch tube which is the spacing between tubes from center to center and the longitudinal tube pitch (P_l) can be ignored since there is only one row. The transverse pitch length is defined:

$$P_t = D_f + f_s \quad (8)$$

where the f_s is the fin spacing.

3.1.1 Serrated helical fins

By increasing the surface area you are in effect increasing the capacity of the heat exchanger to transfer heat, but it is limited to the thermal conductivity and geometry of the fins, decreasing thermal conductivity would mean a decrease in fin efficiency thus not as much heat could be transferred, that is why in many ACHE the fins are made of aluminium due to the high thermal conductivity abilities of the aluminium.

The total inside surface area can be found using the following equation:

$$A_i = \pi D_i L N \quad (9)$$

The total outside surface is more complicated due to the helical serrated fin geometry but following equation determines the surface area [23]:

$$\frac{A_{o,serr}}{LN} = \pi D_o(1 - n_f t_f) + 0,01016\pi n_f(D_o + 0,00508) + \pi n_f(D_o + 0,00508) \cdot [(2l_f - 0,01016) \cdot (w_s + t_f) + w_s t_f] \quad (10)$$

Prime outside surface area, which is the visible part of the tube with fins, is as follows:

$$\frac{A_{po}}{LN} = \pi D_o(1 - n_f t_f) \quad (11)$$

The cross sectional net free area where the air flows across one row is found by the following equations:

$$\frac{A_c}{LN_t} = (D_o + 2l_f t_f n_f) \quad (12)$$

$$A_n = WL - A_c LN_t \quad (13)$$

where the N_t is the number of tubes per each row.

Thus we can define our mass velocity based on the net free area available:

$$G_n = \frac{\dot{m}_{air}}{A_n} \quad (14)$$

From there we can determine our Reynolds number for the air as:

$$Re_{air} = \frac{G_n D_o}{\mu_b} \quad (15)$$

3.1.2 Solid helical fins

As mentioned during the discussion of serrated type fins the surface area is of utmost importance when it comes to ACHE performance. However the heat transfer coefficient is also affected by the geometry and the turbulence effects that are present as air flows across tubes, the serrated fins induce more turbulence hence the heat transfer is more effective than the solid fins. But the pressure loss is also increased by using serrated fins, there are more obstructions for the air rather than for solid helical fins.

The internal surface area of the solid fin type does not change and can be viewed in Equation (9) but the external surface as is as follows:

$$\frac{A_{o,solid}}{LN} = \pi D_o(1 - n_f t_f) + \pi n_f [2l_f(D_o + l_f) + t_f(D_o + 2l_f)] \quad (16)$$

Other factors such as the prime area (Equation 11), cross sectional net free area (Equations 12,13), mass flux (Equation 14) and Reynolds number (Equation 15) remain the same.

3.2 Heat transfer approach

3.2.1 Internal heat transfer correlations

Various correlations exist for turbulent internal flow heat transfer coefficients in our case Gnielinski correlation [24] was chosen and it is defined as:

$$\text{Nu}_s = \frac{(f/8)(\text{Re}_s - 1000)\text{Pr}_s}{1 + 12.7(f/8)^{1/2}(\text{Pr}_s^{2/3} - 1)} \quad (17)$$

and is valid for [25]:

$$\begin{aligned} 0,5 &\leq \text{Pr}_s \leq 2000 \\ 3000 &\leq \text{Re}_s \leq 5 \times 10^6 \end{aligned}$$

The Gnielinski correlation is an assumption that the flow does not move into the two-phase region in such a way that it affects the internal heat transfer coefficient in a dramatic way. There won't be any annular fluid film formulation in the tube banks, the steam is assumed to be dry steam. Other factors such as the effect of non-condensable gases on the heat transfer coefficient will be negligible, the effect of the internal heat transfer coefficient is relatively small compared to the external heat transfer coefficient for the ACHE. Two-phase flow correlations were looked at such as Shah (2009) correlation which is an improved version of the Shah (1979) correlation [26] [27]. Decision was made to assume a single phase flow due to lack of data and uncertainties in the correlation and relatively low steam quality changes through the ACHE.

The Reynolds number can be determined by the following equation:

$$\text{Re}_s = \frac{\rho_s v_s D_i}{\mu_s} \quad (18)$$

where as the Nusselt number is defined as:

$$\text{Nu}_s = \frac{h_i D_i}{k_s} \quad (19)$$

The Prandtl number is defined:

$$\text{Pr}_s = \frac{c_{p,s} \mu_s}{k_s} \quad (20)$$

usually the Prandtl number is given in tables.

The friction factor is defined by Colebrook-White [28]:

$$\frac{1}{\sqrt{f}} = -2,0 \log \left[\frac{\delta/D_i}{3,7} + \frac{2,51}{\text{Re}_s \sqrt{f}} \right] \quad (21)$$

where δ is the roughness of the pipe.

Equations (17, 18, 19, 20 and 21) are used to determine the h_i which is the internal heat transfer coefficient for the steam.

3.2.2 External heat transfer correlations

Again multiple variations of correlations exist to determine the heat transfer coefficient for external flow, it is highly dependant upon behaviour of the flow and the geometry the flow passes. The correlation chosen to examine further was the ESCOA (Extended Surface Corporation of America) correlation because the validity of the correlation covers the range in which the Reynolds number for our problem is in. The correlation covers serrated finned helical geometry, external heat transfer coefficient and pressure drop correlation, the correlations were originally developed by C. Weierman [29] for ESCOA [23].

The correlations are as follows for the heat transfer coefficient for serrated fins in a staggered arrangement:

$$C_1 = 0,25 \cdot \text{Re}_{air}^{-0,35} \quad (22)$$

$$C_3 = 0,55 + 0,45 \cdot e^{(-0,35 \cdot l_f/s_f)} \quad (23)$$

$$C_5 = 0,7 + \left[0,7 - 0,8 \cdot e^{-0,15 \cdot N_r^2} \right] \cdot e^{(-1,0 \cdot P_t/P_l)} \quad (24)$$

$$j = C_1 \cdot C_3 \cdot C_5 \cdot \left(\frac{D_f}{D_o} \right)^{0,5} \cdot \left(\frac{T_b}{T_s} \right)^{0,25} \quad (25)$$

$$h_c = j \cdot G_n \cdot c_{p,air} \left(\frac{k_b}{c_{p,air} \mu_{air}} \right)^{2/3} \quad (26)$$

$$h_o = \left(\frac{1}{h_c} + R_{fo} \right)^{-1} \quad (27)$$

¹ To determine the effective heat transfer coefficient for the serrated helical fins we need to find the fin efficiency which is defined :

$$b = l_f + \left(\frac{t_f}{2} \right) \quad (28)$$

$$m = \left[h_o \cdot \frac{t_f + w_s}{6k_f t_f w_s} \right]^{0,5} \quad (29)$$

$$X = \frac{\tanh(mb)}{mb} \quad (30)$$

$$E = X(0,9 + 0,1X) \quad (31)$$

Thus we can now determine our effective heat transfer coefficient:

$$h_e = h_o \cdot \left[\frac{E \cdot (A_o - A_{po}) + A_{po}}{A_o} \right] \quad (32)$$

To determine the heat transfer for the solid fins almost all factors as mentioned for serrated fins stay the same but one factor C_3 changes since it is geometry related:

$$C_3 = 0,35 + 0,65 \cdot e^{(-0,25 \cdot l_f/s_f)} \quad (33)$$

¹ Equations 28-30 and 34-36 requires the use of Imperial units, all length units need to be in inches and heat transfer coefficients need to be represented as Btu/hr-ft²-F to get the correct efficiency.

² The effectiveness is a different approach altogether and is as such :

$$b = l_f + \left(\frac{t_f}{2} \right) \quad (34)$$

$$m = \left[\frac{h_o}{6k_f t_f} \right]^{0,5} \quad (35)$$

$$X = \frac{\tanh(mb)}{mb} \quad (36)$$

$$Y = X(0,7 + 0,3X) \quad (37)$$

$$E = Y \left[0,45 \ln \left(\frac{D_f}{D_o} \right) \cdot (Y - 1) + 1 \right] \quad (38)$$

The ESCOA correlation have measurement uncertainty of about $\pm 10\%$ according to Weierman and the range of validity lies [29]:

$$\begin{aligned} 2000 &\leq \text{Re}_s \leq 5 \times 10^5 \\ 9,5 \text{ mm} &\leq l_f \leq 38,1 \text{ mm} \\ 0,9 \text{ mm} &\leq t_f \leq 4,2 \text{ mm} \\ 39 \text{ fins/m} &\leq n_f \leq 276 \text{ fins/m} \end{aligned}$$

When all heat transfer coefficients are known we can determine our over all heat transfer coefficient based on the outside surface area, it is also possible to determine it based on the inside surface. Based on the outside surface area the over all heat transfer coefficient is:

$$U_o = \left[\frac{1}{h_e} + \left(\frac{t_w}{k_w} \right) \cdot \left(\frac{A_o}{A_i} \right) + \left(\frac{1}{h_i} + R_{fi} \right) \cdot \left(\frac{A_o}{A_i} \right) \right]^{-1} \quad (39)$$

Note: The fouling on the outside (R_{fo}) is included in the effective heat transfer coefficient for the air side.

The fouling factors are obtained through TEMA standard and written literature, although the external fouling factor is not as important as the internal fouling factor due to the low heat transfer coefficient on the air side. The internal and external fouling factors are selected to be 0,00009 and 0,00035 $\text{m}^2\text{-K/W}$ respectively. [6]

Now it is possible to revert back to Equation (6) to determine the over all heat transfer coefficient for the heat exchanger since the surface area outside and inside the tubes is known.

² Equations 28-30 and 34-36 requires the use of Imperial units, all length units need to be in inches and heat transfer coefficients need to be represented as $\text{Btu/hr-ft}^2\text{-F}$ to get the correct efficiency.

3.3 Pressure drop correlation

The total pressure drop across the fan governs the selection of motor and fans, there for it is an important factor in determining the overall energy consumption of the ACHE. The power required is determined by the following equations:

$$\Delta P = \Delta P_f + \frac{\rho_1 V_{fan}^2}{2} \quad (40)$$

$$W_{fan} = \frac{G_n \cdot A_n \cdot \Delta P}{\eta_{fan} \cdot \rho_b} \quad (41)$$

$$W_{motor} = \frac{W_{fan}}{\eta_{motor}} \quad (42)$$

where the first term ΔP_f is the static pressure drop across the bundle and the second term is the velocity pressure those two terms give the total pressure drop. [30]

3.3.1 Serrated tube banks

To find the pressure drop for serrated finned tubing in staggered arrangement we have [23]:

$$C_2 = 0,07 + 8,0 \text{Re}_{air}^{-0,45} \quad (43)$$

$$C_4 = 0,11 [0,05 \cdot P_t/D_o]^{-0,7 \cdot (l_f/s_f)^{0,23}} \quad (44)$$

$$C_6 = 1,1 + \left[1,8 - 2,1 e^{-0,15 N_r^2} \right] \left[e^{-2,0 P_l/P_t} \right] - \left[0,7 - 0,8 e^{-0,15 N_r^2} \right] \left[e^{-0,6 P_l/P_t} \right] \quad (45)$$

$$f = C_2 \cdot C_4 \cdot C_6 \cdot \left(\frac{D_f}{D_o} \right)^{0,5} \quad (46)$$

$$\beta^2 = \left(\frac{A_n}{W \cdot L} \right)^2 \quad (47)$$

$$a = \left(\frac{1 + \beta^2}{4 \cdot N_r} \right) \cdot \rho_b \cdot \left(\frac{1}{\rho_2} - \frac{1}{\rho_1} \right) \quad (48)$$

$$\Delta P_f = (f + a) \cdot \frac{2 \cdot G_n^2 \cdot N_r}{\rho_b} \quad (49)$$

3.3.2 Solid tube banks

We use the same equations as for the serrated fins except for one change in the geometry factor:

$$C_4 = 0,11 [0,05 \cdot P_t/D_o]^{-0,7 \cdot (l_f/s_f)^{0,20}} \quad (50)$$

Apart from Equation 44, Equations 43 to 49 are valid for solid finned tubes.

3.4 Concentration of TDS in the carryover

To dilute the concentration of TDS from the separator the ACHE condenses the steam partially to increase the size of the droplets and capture smaller droplets that are in the way, by introducing the flow to highly turbulent situation the droplets are mixed in the process and effectively dilutes the concentration of TDS contained with the carryover brine.

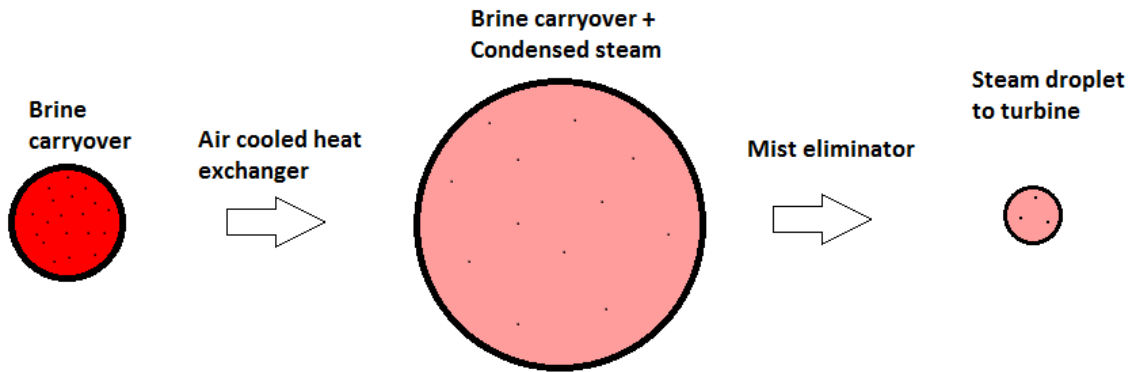


Figure 14: Steam droplet from the separator being condensed via the ACHE and through the mist eliminator

As Figure 14 depicts the brine carryover droplet is enlarged by the condensing steam in the ACHE thus the TDS within the brine carryover is diluted by the amount of steam condensed and as mentioned earlier by mixing the flow effectively the TDS is reduced that would otherwise be sent through the turbine, final stage is removal of the larger droplets through the mist eliminator.

As mentioned earlier there are two factors governing the condensate generation, thermal losses and the pressure loss. The method used is from Russel James's approach in Wairakai, New Zealand [19]. The fraction of the total flow (excluding NCG's) that is

condensate is then the following:

$$\gamma_{th} = \frac{Q}{\dot{m}_s \cdot h_{fg}} \quad (51)$$

We need to determine the saturated vapour enthalpy at the pressure after the ACHE and accounting for the pressure drop as an example, if the pressure drop is 0,1 bar and our initial working pressure is 10 bar we will determine the vapour enthalpy at 9,9 bar and our evaporation due to the pressure drop becomes:

$$\gamma_p = \frac{h_g - h_{gp}}{h_{fg}} \quad (52)$$

where h_g is the vapour enthalpy before the ACHE process and h_{gp} is the vapour enthalpy after the ACHE.

Subtracting the condensation fraction and the evaporation fraction we get the true wetness fraction:

$$\gamma_t = \gamma_{th} - \gamma_p \quad (53)$$

So our true condensation generation is:

$$\dot{m}_{cond} = \dot{m}_s \cdot \gamma_t \quad (54)$$

Once we know how much fluid is truly condensed and mixes with the carryover droplets, which is highly concentrated with TDS, we can determine how much of the TDS has been diluted.

The brine carryover:

$$\dot{m}_{br} = \dot{m}_s \cdot (1 - x_1) \quad (55)$$

Initial carryover vs the condensed steam:

$$\alpha = \frac{\dot{m}_{br}}{\dot{m}_{cond}} \quad (56)$$

The amount of TDS after the dilution by the condensed steam then becomes:

$$\text{TDS}_d = \text{TDS}_{init} \cdot \alpha \quad (57)$$

This method can then be continued through out to the demister to find the final concentration of TDS that goes through the turbine, however it is necessary to know the quality of the steam coming out of the demister to know the TDS of the droplets that goes into the turbine. The process above is a simplification of a much more complicated process and the assumption is that all of the chemicals present are trapped in the brine and no chemical reactions are taking place between the mediums.

3.5 Computational Fluid Dynamics

Computational Fluid Dynamics (CFD) analysis was performed using the Autodesk Simulation 2015 software to determine some aspects of the design such as the pressure drop within the ACHE.

Momentum equations written out in the Cartesian coordinate system:

$$\rho \left(\frac{\partial u}{\partial t} + u \frac{\partial u}{\partial x} + v \frac{\partial u}{\partial y} + w \frac{\partial u}{\partial z} \right) = -\frac{\partial p}{\partial x} + \mu \left(\frac{\partial^2 u}{\partial x^2} + \frac{\partial^2 u}{\partial y^2} + \frac{\partial^2 u}{\partial z^2} \right) + \rho g_x \quad (58)$$

$$\rho \left(\frac{\partial v}{\partial t} + u \frac{\partial v}{\partial x} + v \frac{\partial v}{\partial y} + w \frac{\partial v}{\partial z} \right) = -\frac{\partial p}{\partial y} + \mu \left(\frac{\partial^2 v}{\partial x^2} + \frac{\partial^2 v}{\partial y^2} + \frac{\partial^2 v}{\partial z^2} \right) + \rho g_y \quad (59)$$

$$\rho \left(\frac{\partial w}{\partial t} + u \frac{\partial w}{\partial x} + v \frac{\partial w}{\partial y} + w \frac{\partial w}{\partial z} \right) = -\frac{\partial p}{\partial z} + \mu \left(\frac{\partial^2 w}{\partial x^2} + \frac{\partial^2 w}{\partial y^2} + \frac{\partial^2 w}{\partial z^2} \right) + \rho g_z \quad (60)$$

Continuity equation based on incompressible flow:

$$\frac{\partial u}{\partial x} + \frac{\partial v}{\partial y} + \frac{\partial w}{\partial z} = 0 \quad (61)$$

The energy equation which usually follows the momentum and continuity equations is decoupled from the system since the viscosity is assumed to be constant through out the system and there is no heat transfer in the analysis.

For comparison sake two turbulence models were used to determine the pressure drop, k- ϵ and the SST k- ω . The results from those two models will be compared later on.

3.5.1 K- ϵ Turbulence Model

The k- ϵ model is defined from Launder and Spalding [31].

The turbulent kinetic energy equation:

$$\frac{\partial(\rho k)}{\partial t} + \frac{\partial(\rho k u_i)}{\partial x_i} = \frac{\partial}{\partial x_j} \left[\frac{\mu_t}{\sigma_k} \frac{\partial k}{\partial x_j} \right] + 2\mu_t E_{ij} E_{ij} - \rho \epsilon \quad (62)$$

The specific dissipation rate:

$$\frac{\partial(\rho \epsilon)}{\partial t} + \frac{\partial(\rho \epsilon u_i)}{\partial x_i} = \frac{\partial}{\partial x_j} \left[\frac{\mu_t}{\sigma_\epsilon} \frac{\partial \epsilon}{\partial x_j} \right] + C_{1\epsilon} \frac{\epsilon}{k} 2\mu_t E_{ij} E_{ij} - C_{2\epsilon} \rho \frac{\epsilon^2}{k} \quad (63)$$

Kinematic Eddy Viscosity:

$$\mu_t = \rho C_\mu \frac{k^2}{\epsilon} \quad (64)$$

The constants for the model are defined as follows [32]:

$$\begin{aligned} C_\mu &= 0,09 & \sigma_k &= 1,00 & \sigma_\epsilon &= 1,30 \\ C_{1\epsilon} &= 1,44 & C_{2\epsilon} &= 1,92 \end{aligned}$$

3.5.2 SST K- ω Turbulence Model

The SST k- ω model [33] is combination of the Wilcox k- ω model [34] and the standard k- ϵ model and is as follows. The turbulence kinetic energy equation:

$$\frac{\partial k}{\partial t} + U_j \frac{\partial k}{\partial x_j} = P_k - \beta^* k \omega + \frac{\partial}{\partial x_j} \left[(\nu + \sigma_k \nu_t) \frac{\partial k}{\partial x_j} \right] \quad (65)$$

The specific dissipation rate:

$$\frac{\partial \omega}{\partial t} + U_j \frac{\partial \omega}{\partial x_j} = \alpha S^2 - \beta \omega^2 + \frac{\partial}{\partial x_j} \left[(\nu + \sigma_\omega \nu_t) \frac{\partial \omega}{\partial x_j} \right] + 2(1 - F_1) \sigma_{\omega 2} \frac{1}{\omega} \frac{\partial k}{\partial x_i} \frac{\partial \omega}{\partial x_i} \quad (66)$$

Kinematic Eddy Viscosity:

$$\nu_t = \frac{a_1 k}{\max(a_1 \omega, SF_2)} \quad (67)$$

The two blending functions which govern the free stream region and the inside of the boundary layer ($F_1 = 1$, inside the boundary layer and $F_1 = 0$, in the free stream.)

$$F_1 = \tanh \left\{ \left\{ \min \left[\max \left(\frac{\sqrt{k}}{\beta^* \omega y}, \frac{500\nu}{y^2 \omega} \right), \frac{4\sigma_{\omega 2} k}{CD_{k\omega} y^2} \right] \right\}^4 \right\} \quad (68)$$

$$F_2 = \tanh \left[\left[\max \left(\frac{2\sqrt{k}}{\beta^* \omega y}, \frac{500\nu}{y^2 \omega} \right) \right]^2 \right] \quad (69)$$

$$CD_{k\omega} = \max \left(2\rho\sigma_{\omega 2} \frac{1}{\omega} \frac{\partial k}{\partial x_i} \frac{\partial \omega}{\partial x_i}, 10^{-10} \right) \quad (70)$$

$$P_k = \min \left(\tau_{ij} \frac{\partial U_i}{\partial x_j}, 10\beta^* k \omega \right) \quad (71)$$

where the constants for the model are defined [35]:

$$\begin{aligned} \alpha_1 &= \frac{5}{9} & \alpha_2 &= 0.44 \\ \beta_1 &= 0,075 & \beta_2 &= 0.0828 \\ \beta^* &= 0,09 & \sigma_{k1} &= 0.85 \\ \sigma_{k2} &= 1 & \sigma_{\omega 1} &= 0.5 \\ \sigma_{\omega 2} &= 0.856 \end{aligned}$$

3.6 Reaction forces due to thermal expansion

During start up, the steam travels through the pipes and the ACHE warms up, due to the large temperature difference a significant amount of thermal expansion is expected, the reaction forces on the flanges will be examined.

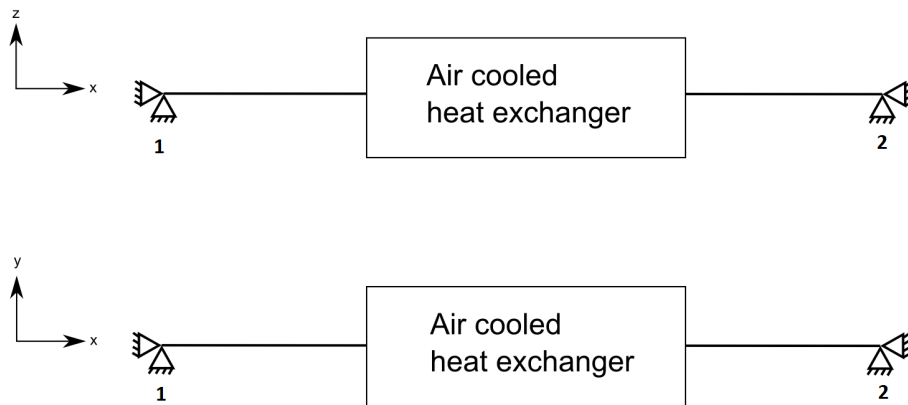


Figure 15: Free body diagrams of the reaction forces due to thermal expansion.

As Figure 15 shows the setup for the analysis, determining the reaction forces of the thermal expansion.

$$\sum F_x = R_{x1} + R_{x2} - \sum F_{x,exp} = 0 \quad (72)$$

$$\sum F_y = R_{y1} + R_{y2} - \sum F_{y,exp} = 0 \quad (73)$$

$$\sum F_z = R_{z1} + R_{z2} - \sum F_{z,exp} = 0 \quad (74)$$

$$\sum M = 0$$

from where the summation of $F_{i,exp}$ (where i denotes the direction) are the forces generated due to the thermal expansions within the model.

The magnitude of those forces are defined as:

$$R_1 = \sqrt{R_{x1}^2 + R_{y1}^2 + R_{z1}^2} \quad (75)$$

$$R_2 = \sqrt{R_{x2}^2 + R_{y2}^2 + R_{z2}^2} \quad (76)$$

where R denotes the reaction force and subscripts indicate direction and location. Thermal expansion is a factor that the designer needs to be aware of, the forces exerted from a material that undergoes thermal expansion can be huge. There for it is important to evaluate the reaction forces produced by the expansion.

A finite element software (Autodesk Simulation Mechanical 2015 R1) was used to find those reaction forces exerted by the change in temperature.

3.7 Uncertainty propagation

To determine the final design from variables that might not be fairly accurate an uncertainty propagation was done to view how sensitive the final solution is to dynamic situations. The simplified uncertainty propagation is defined as:

$$U_y = \sqrt{\sum_i \left(\frac{\partial Y}{\partial X_i} \right)^2 \cdot U_{x_i}^2} \quad (77)$$

where U_y is the uncertainty of the variable y denoted in the subscript and U_{x_i} is the standard deviation of X_i . The assumption has to be made that the individual measurements are uncorrelated and random. [36]

An example is that you would take the partial derivative of the heat transferred Q with respect to a variable that might be changing such as atmospheric pressure, some measurements were made over a period of time to determine the standard deviation of the atmospheric pressure data by using that the uncertainty of the heat transfer with respect to the changing atmospheric pressure measurements can be determined.

Chapter 4

Results

4.1 Analytical model

A model was built in EES to determine various factors such as how face velocity affects the condensation rate within the ACHE among others.

The model takes into account the following parameters:

- Elevation changes / atmospheric pressure.
- Steam properties entering the ACHE.
- Geometry of the finned tubing, number of tubes and rows.
- Material properties such as conductivity, fouling and wall roughness.
- Condensation due to thermal losses and evaporation due to pressure losses.
- Outside conditions such as relative humidity and temperature.
- Steam purity entering the turbine with and without the ACHE given the TDS from the separator.
- Fan sizing and power consumption.

The model is bound by limits that were described earlier such as fin height, thickness, number of fins and the Reynolds number. In the upcoming section it is necessary to be aware of these limits.

A set of base conditions have been set and are found in Table 2 and they can all be changed accordingly.

Table 2: ACHE initial conditions and assumptions

State	Value
<i>Efficiencies:</i>	
Fan and motor efficiency	58%
<i>Environment:</i>	
Maximum ambient temperature	30°C
Average atmospheric pressure	0,95 bar _a
Relative humidity	80%
<i>Initial internal fluid state:</i>	
Pressure	10 bar _a
Quality	99,99%
Total mass flow	16 kg/s
TDS in the separator	1500 ppm
Internal pressure drop ¹	0,11 bar _a
<i>Geometry:</i>	
Fan diameter	900 mm
Length of tubes	1000 mm
Width of the bundle	1254 mm
Number of rows	1
Number of tubes per row	7
Tubes	5 inch, Sch. 40
Transverse tube pitch	D_{fin} - Fin spacing
<i>Tube properties:</i>	
Thermal conductivity	50 W/m-K
Average wall roughness	0,0457 mm
Average internal velocity	34,5 m/s
Inside fouling factor	90 mm ² -K/W
Internal pressure drop	0,11 bar _a
<i>Fin properties:</i>	
Fin thermal conductivity	50 W/m-K
External fouling factor	350 mm ² -K/W

¹ The internal pressure drop is defined more accurately in the coming chapter under CFD model.

A few assumptions that are necessary to be aware of:

- Air flow across the tubes is uniform
- NCG gas is considered inert and is not accounted for
- No air recirculation at the fan outlet
- Heat loss from the headers to the environment are not considered

The model interface is shown on Figure 16.

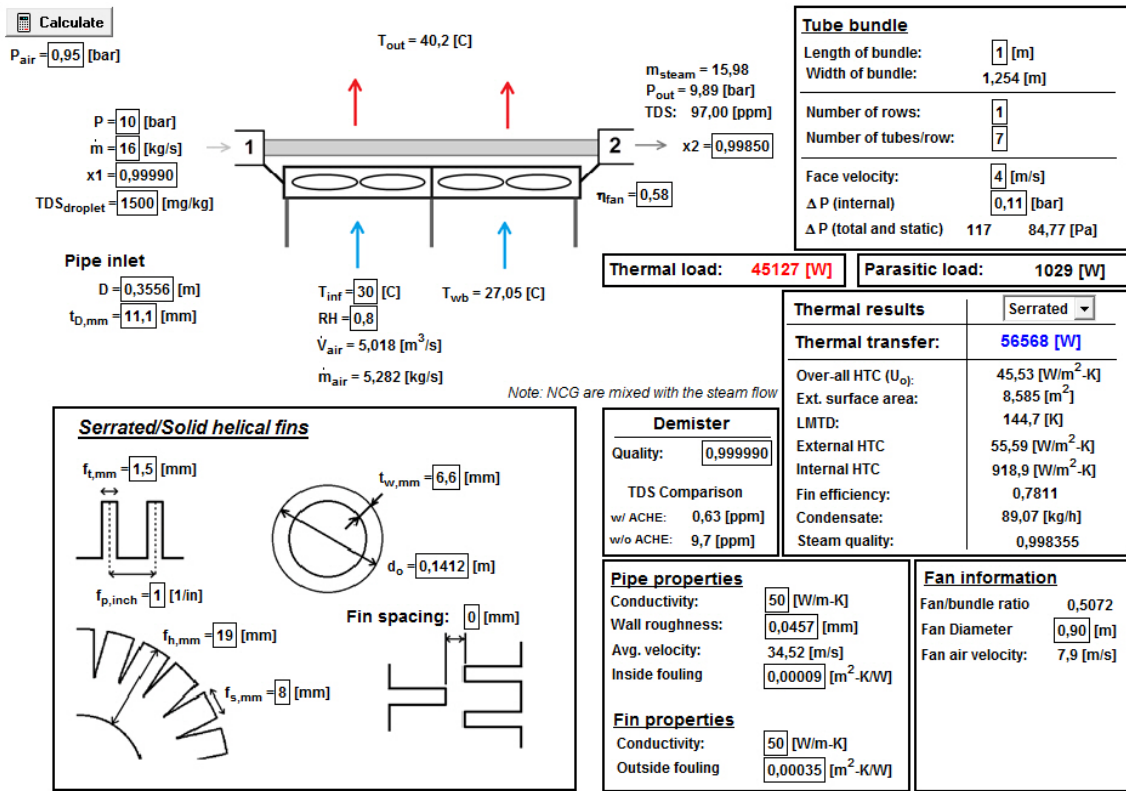


Figure 16: EES Model interface for the base variables

4.1.1 Design scenarios

First the idea is to introduce the model with its base values then from there on we will look at changing aspects of the model. First we will introduce the difference between serrated and solid fins for varying face velocities. Refer to Table 2 and 3 for parameters.

Table 3: Ranges for the changing ACHE variables and the fixed base variables

ACHE variables	Scenario variables	Base scenario
Fin height	9,5 - 38,1 mm	19 mm
Fin thickness	1,0 - 2,0 mm	1,5 mm
Fins per meter	39 - 276 fins/m	39,4 fins/m
Segment width	4,5 - 8,0 mm	8,0 mm
Fin spacing ¹	0 - 10 mm	0 mm
Inside fouling factor	0 - 6000	90 mm ² ·K/W
External fouling factor	0 - 6000	350 mm ² ·K/W

¹ Fin spacing is the transverse distance between fins in the same tube row. (See Figure 16 for clarification)

Base scenario

The base scenario is a sample of the models capabilities. Values are chosen and fixed the only changing factor is the velocity across the tube bundle since it is the only factor that affects the thermal transfer, assuming fixed outside temperature.

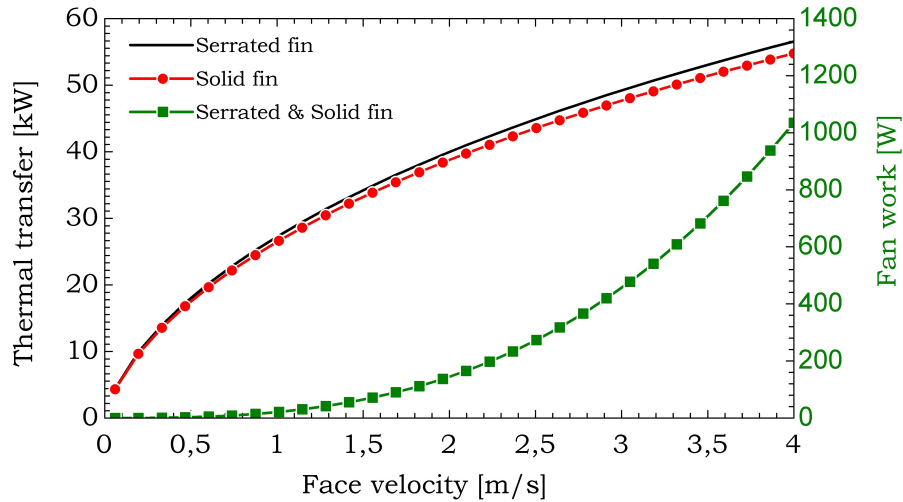


Figure 17: Thermal transfer & fan work as a function of face velocity

On Figure 17 the difference between the work performed by the fan for serrated or solid fins is so small that it is considered to be the same.

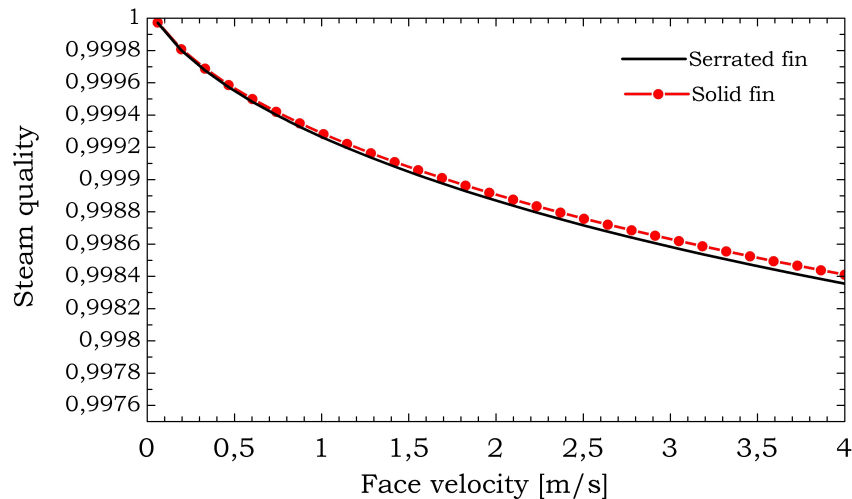


Figure 18: Steam quality for serrated and solid fins as a function of face velocity

To view the capabilities of the model further we will introduce two different design scenarios. Scenario A is where we have the maximum temperature for that given location,

Scenario B is a very cold scenario. Due to the multi-variable options in the model the variables that are not being looked at remain fixed and based on the base scenario while the changing variable can vary according to Table 3.

Table 4: Design scenarios

Design scenarios	Scenario A	Scenario B
Face velocity	4 m/s	2,5 m/s
Outside temperature	30°C	0°C

The face velocities are selected from common face velocities, the literature says 1,5 - 3,6 m/s is common and the velocity in the fan should be around 3,8 - 10,2 m/s [37]. These values are conservative and depending on if you have induced or forced draft configuration, 4 m/s face velocity was chosen for Scenario A as the worst case.

Scenario A

Table 5: Results from Scenario A

Variable	Serrated fins	Solid fins
Thermal transfer	56.568 W	54.765 W
Parasitic load	1029 W	1035 W
Temp. in	30°C	30°C
Temp. out	40,2°C	39,9°C
LMTD	144,7°C	144,9°C
Condensate rate	89,1 kg/hr	85,9 kg/hr
Steam quality	0,99836	0,99841
Airside static pressure drop	84,8 Pa	85,5 Pa
Airside total pressure drop	117 Pa	117,7 Pa
TDS droplet concentration ¹	0,67 ppm	0,68 ppm
TDS droplet w/o the ACHE	9,7 ppm	10,1 ppm

1. Based on demister outlet steam quality of 99,999%

Fin height: In Appendix A on Figure 28 shows how the thermal transfer and fan work changes with changing fin height, note that the transverse tube pitch is directly related to the fin height through fin spacing variable.

Fin thickness: As seen In Appendix A on Figure 29 the fin thickness affects the thermal transfer, the thicker the fin the more heat is transferred due to conductivity, the outside

surface area of the ACHE is increasing which results in more heat being transferred. There is a slight increase in the fan work but it is insignificant.

Fins per meter: In Appendix A on Figure 30 the fins per meter factor is one of the most important factors as it can increase the thermal transfer rate by more than two folds, but it also increases the power the fan needs due to the increased pressure static pressure drop across the tube bundle. Another factor of having increased fins per meter is fouling and cleaning, very tightly packed fins have a tendency to capture small dust particles and they cluster together there decreasing the performance of the heat exchanger via external fouling.

Fin spacing: In Appendix A on Figure 31 it can be seen that the work done by the fan is affected by the fin spacing, the reason behind that is that the fin spacing factor is directly related to the spacing between the tubes. Thus when we have small fins the distance between the tubes is minimal resulting in high static pressure drop across the bundle. Therefore as the fin height increases so does the spacing between the tubes. The fin spacing indicates how far the end of the fin is from the next fin on the next tube.

Fouling factors: In Appendix A on Figure 32, note the slopes of the lines, they are an indicator on how fast the fouling is affecting the thermal transfer, as depicted by the figure the internal fouling factor has a significant larger slope than the external factor which results in a faster decrease of performance for the heat exchanger. It is however very difficult to select a proper fouling factor, therefore the TEMA standards are often used or specified by clients to be used. The base scenario is based on the TEMA standards for fouling.

Scenario B

Scenario B detailed setup can be viewed in Table 2, 3 and 4. It is set up as a cold scenario.

Not much difference is between Scenario A and B, the reason behind that is the velocity difference between those two scenarios, the fan is controlling the condensing rate of the steam. The most important factor is to know the highs and lows of the temperature variations at the site the device will be located from there the geometry is decided.

Results from Scenario B is plotted in Appendix B same way as Scenario A.

Table 6: Results from Scenario B

Variable	Serrated fins	Solid fins
Thermal transfer	54,805 W	53,116 W
Parasitic load	309,5 W	310,9 W
Temp. in	0°C	0°C
Temp. out	14,3°C	13,9°C
LMTD	172,6°C	172,8°C
Condensate rate	85,92 kg/hr	82,91 kg/hr
Steam quality	0,99841	0,99846
Airside static pressure drop	41,54 Pa	41,82 Pa
Airside total pressure drop	55,82 Pa	56,11 Pa
TDS droplet concentration ¹	0,67 ppm	0,72 ppm
TDS droplet w/o the ACHE	10,06 ppm	10,42 ppm

1. Based on demister outlet steam quality of 99,999%

4.2 CFD model

Four different designs were analysed (see on Figure 19) with the CFD software to determine the pressure drop, due to the irregular geometry.

Design 1 : The original design, 14" inlet pipe distributed in a small header then from the header to the tube banks which are 5" tubes at their end there is a 14" outlet header connected tangential to the tube bank.

Design 2: 14" inlet pipe to a header that has been extended by 2 cm in all directions. 16" outlet header with a reducer to a 14" pipe.

Design 3: 14" inlet to the same header from Design 2, to a 16" end header with two outlets and a reducer from 16" to 7" piping.

Design 4: Same as Design 2 but with a different inlet header as an experiment to see if pressure drop would change.

As can be seen on Figure 20 the design was made as standardized as possible, the front header is designed to API Standard 661/ISO 13706:2001 and the flanges are ASME B16.5 flanges class 150 flanges, however for more safety class 300 can be adopted. [38]

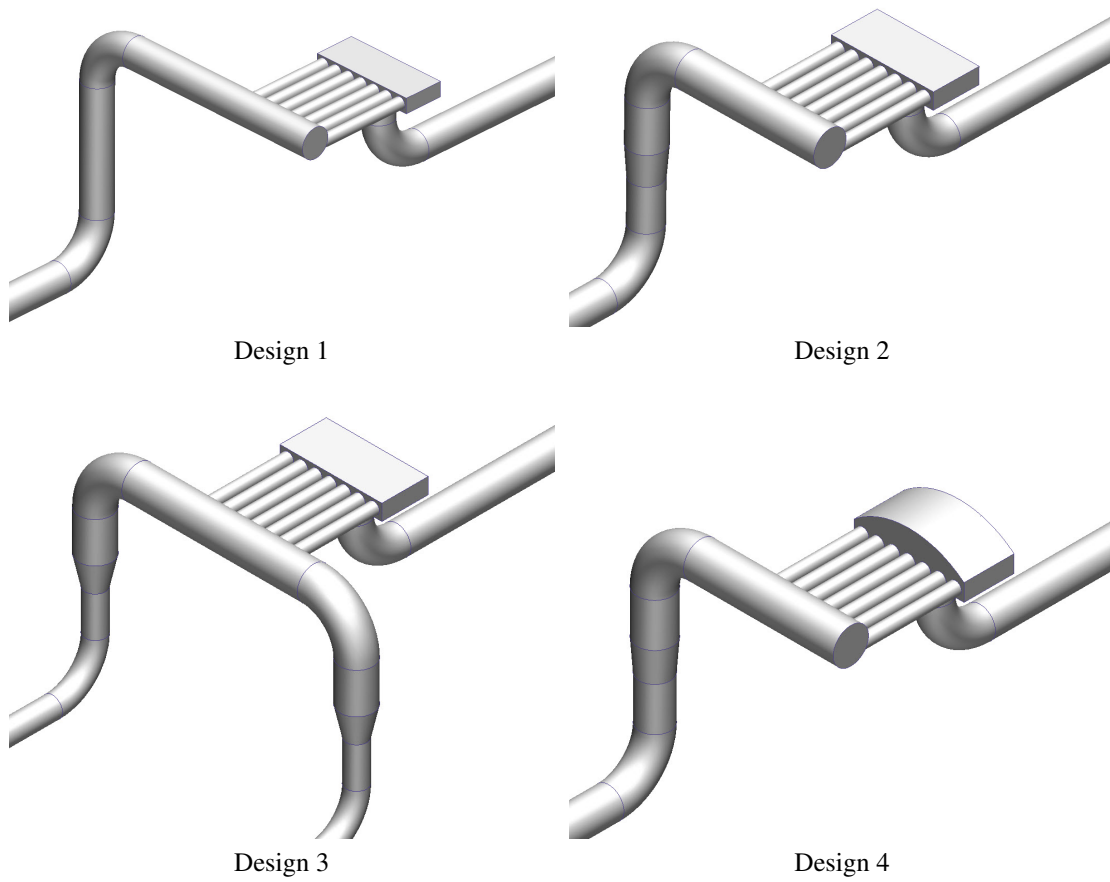


Figure 19: Fluid geometry of the different models

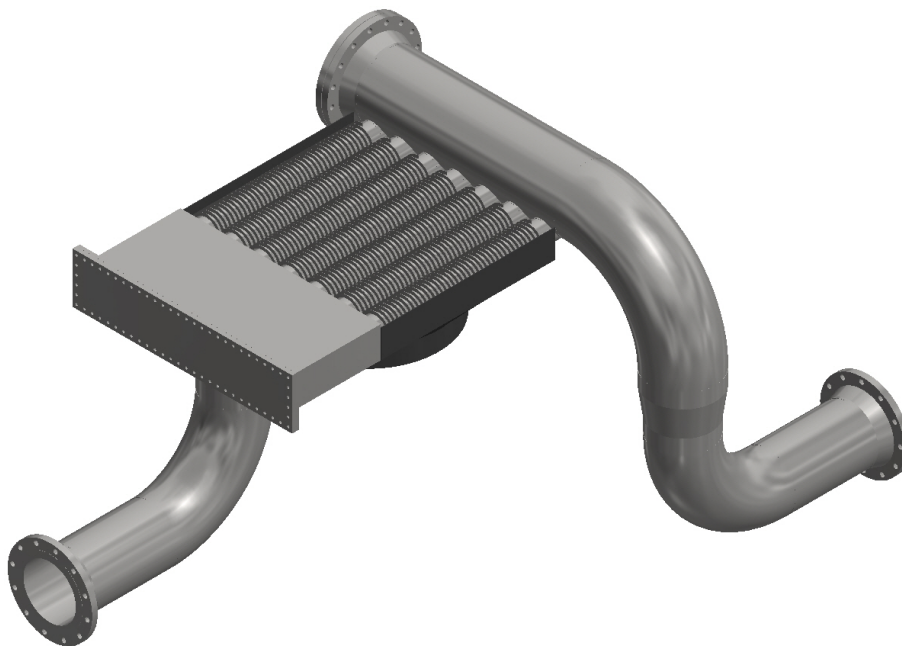


Figure 20: Design 2 without the fluid domain

Two turbulence models were compared, the $k-\epsilon$ and the SST $k-\omega$ models. Enhancements were made to capture the flow better, such as enhancement layering that is especially important for the SST $k-\omega$ since that turbulence model captures more how the flow behaves in the boundary layers, which is the most important factor when analysing pressure drop. The $k-\epsilon$ works also well when determining pressure drop as the results show.

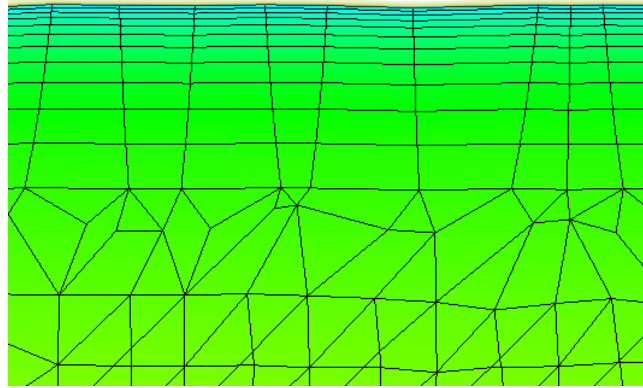


Figure 21: Enhancement layering to capture the effects in the boundary layer regime [9]

The enhanced layering was set as 12 layers, with 1.3 graduation and 0.6 layer factor as is depicted by Figure 21.

The velocity profile at the boundary layer is depicted in Figure 22, note the viscous boundary layer transitions to the turbulence generation layer and then on to the free stream region. The SST $k-\omega$ captures the boundary layer transition more accurately.

Table 7: CFD model details and pressure drop results

Variable	Design 1	Design 2	Design 3	Design 4
Elements	836.150	710.093	896.256	772.056
Nodes	347.532	288.961	368.448	319.028
SST $K-\omega$ pressure drop [Pa]	12870,7	11590,3	11735,0	11770,4
$K-\epsilon$ pressure drop [Pa]	12907,2	11470,4	11461,4	11689,3

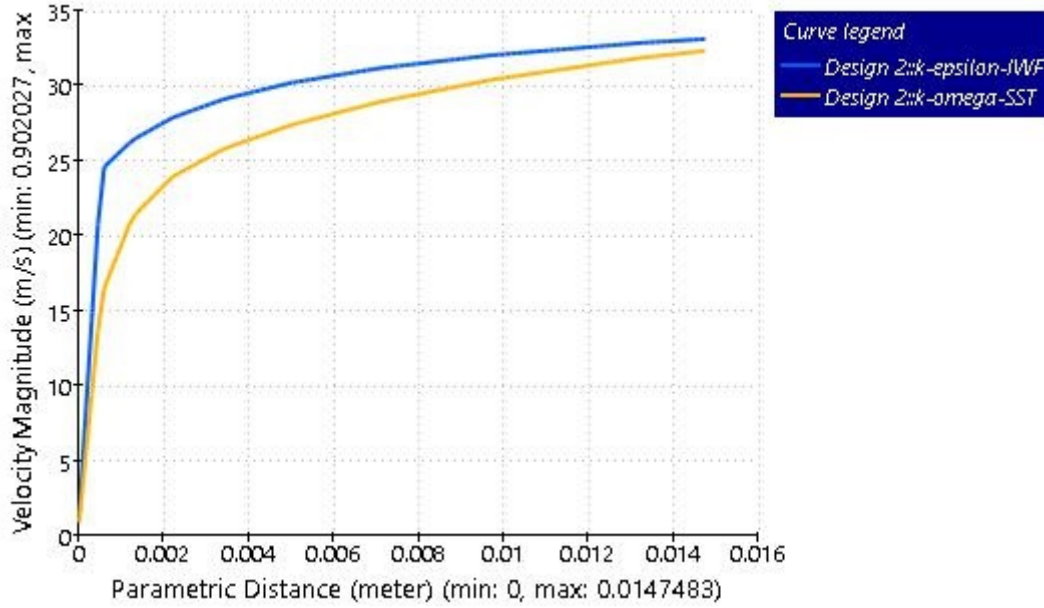


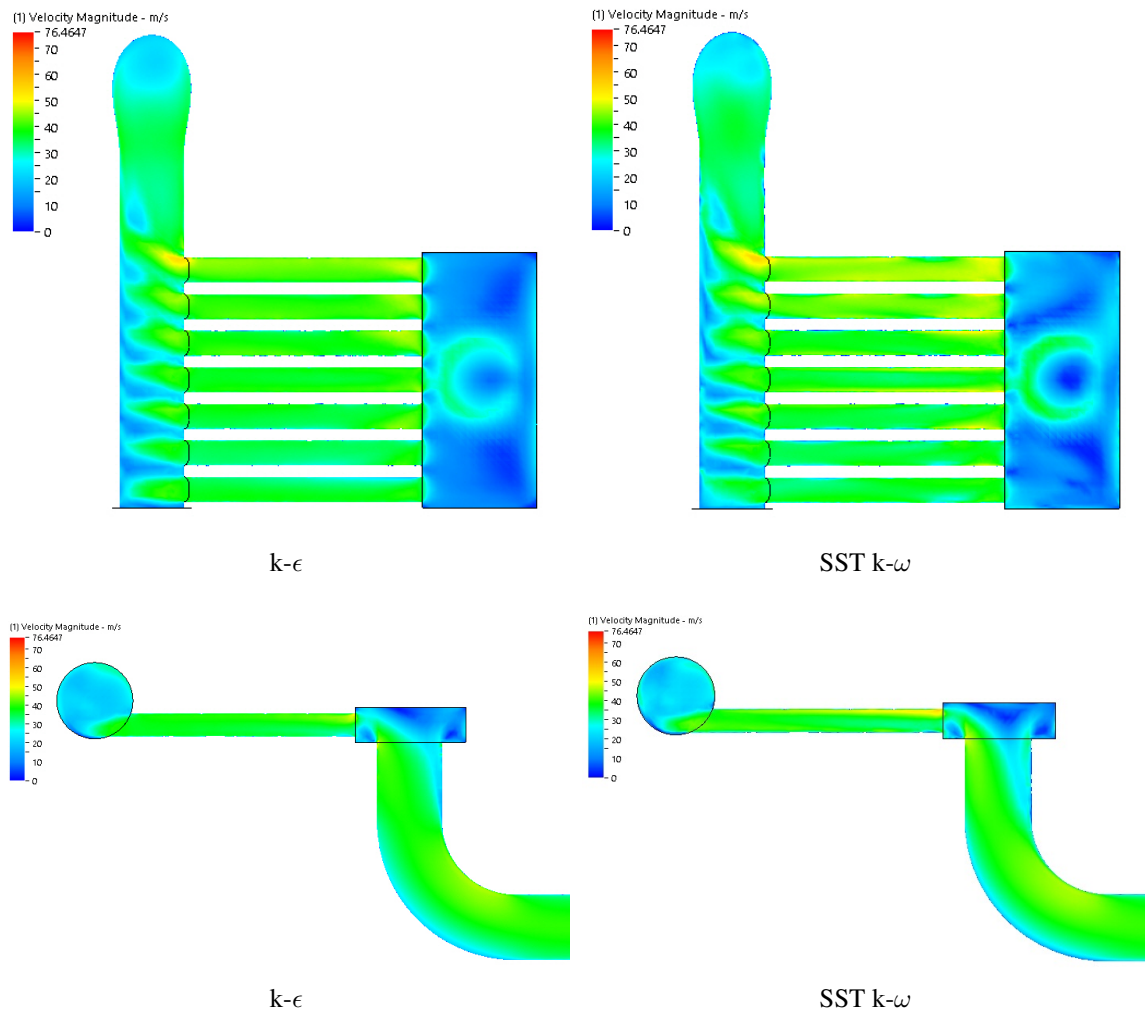
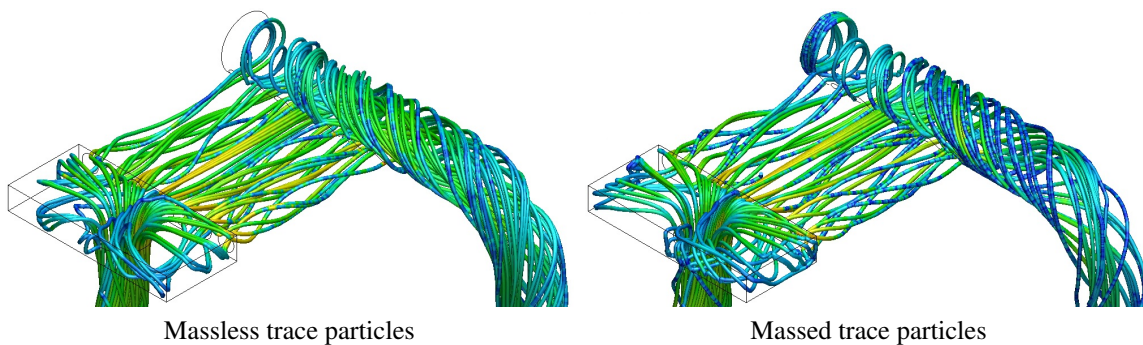
Figure 22: Resultant boundary layer effect from Design 2 near the wall.

There is not much difference between the both turbulence models as can be seen in Table 7, SST $k-\omega$ gives almost the same results as the $k-\epsilon$ for the pressure drop. A visual comparison is shown in Figure 23, the difference is obvious by the boundary layer separation, it is noticeable that the SST $k-\omega$ captures the boundary layer separation more accurately than the $k-\epsilon$. Despite the obvious differences in flow characteristics at the boundary layer the pressure drop remains very similar, for internal flow the accuracy of $k-\epsilon$ does suffice, but to determine more details regarding the flow the SST $k-\omega$ will provide more detail.

As depicted by Figure 24 the traces run through the model and two types are described, that is massless and massed particles. The massed particle was defined in the software as having the density of 1000 kg/m^3 , a diameter of $10 \text{ }\mu\text{m}$ and with the coefficient of restitution of 0,2 [39]. To clarify the coefficient of restitution is the definition on how well the particle is able to bounce off walls and in a sense how it adheres to walls.

An important feature of the design was observed during the CFD analysis. Large formations of vortex swirls were being produced in the tube banks, as the flow enters the first header the flow is divided and the intensity of the flow entering resulted in vortexes forming in such a way that the profile velocity is highly distorted and the flow is adhering to the tube walls, this feature can be observed on Figure 24.

The secondary header acts as a sort of centrifuge, forcing the condensed droplets to adhere to the walls of the header due their momentum, the intensity that occurs in the secondary

Figure 23: Comparison of k- ϵ and SST k- ω on Design 2Figure 24: Trace particle flow for SST k- ω in Design 2

header ensures proper mixing of the steam resulting in condensate that has been diluted due to the steam that has condensed and properly mixed.

Comparison of the other designs are in Appendix C

4.3 Reaction forces

Reaction forces were determined by the usage of Autodesk Simulation Mechanical 2015 R1, these forces are the resultant forces of thermal expansion.

The material used is P235-T1 pipe material for the entire device.

Table 8: Material properties for P235-T1

Density	7850 kg/m ³
Modulus of elasticity	200 GPa
Thermal conductivity	51 W/m-K
Specific thermal capacity	461 J/kg-K
Linear coefficient of thermal expansion	12,9 x 10 ⁻⁶ K ⁻¹

Table is based on information from ThyssenKrupp Materials International, Material Data sheet for P235TR1/2 Grade A and the standard ASTM/ASME A53. Data has been interpolated to fit working temperature of 180°C.

For the P235TR1/2 the material yield strength is generally 235 MPa but it depends on the product thickness and can vary from 235 down to 215 for thicker material. It is assumed the material is homogeneous with an average yield strength of 235 MPa.

As Figure 25 shows is the magnitude of the reaction forces acted upon the flange if it would be totally fixed at that end. This gives an idea on the forces that might be expected from start up to steady state if it would be fixed in that manner. Which is not recommended due to the expansion forces, thus sliding support structures are more appropriate depending on the layout of the plant.

Table 9: Reaction forces (Magnitude)

Variable	Average force
Inlet flange	29,0 kN
Outlet flange	29,4 kN

Von mises stresses are seen on Figure 26 and note that the highest stresses are at the fixed constraints.

Assuming the density of 7850 kg/m³ for the material the total weight of the bare unit (Design 2) without motor and bolts is 1306 kg excluding the fan plenum, bolts, motor and supports. Essentially the total weight of what is depicted in Figure 26.

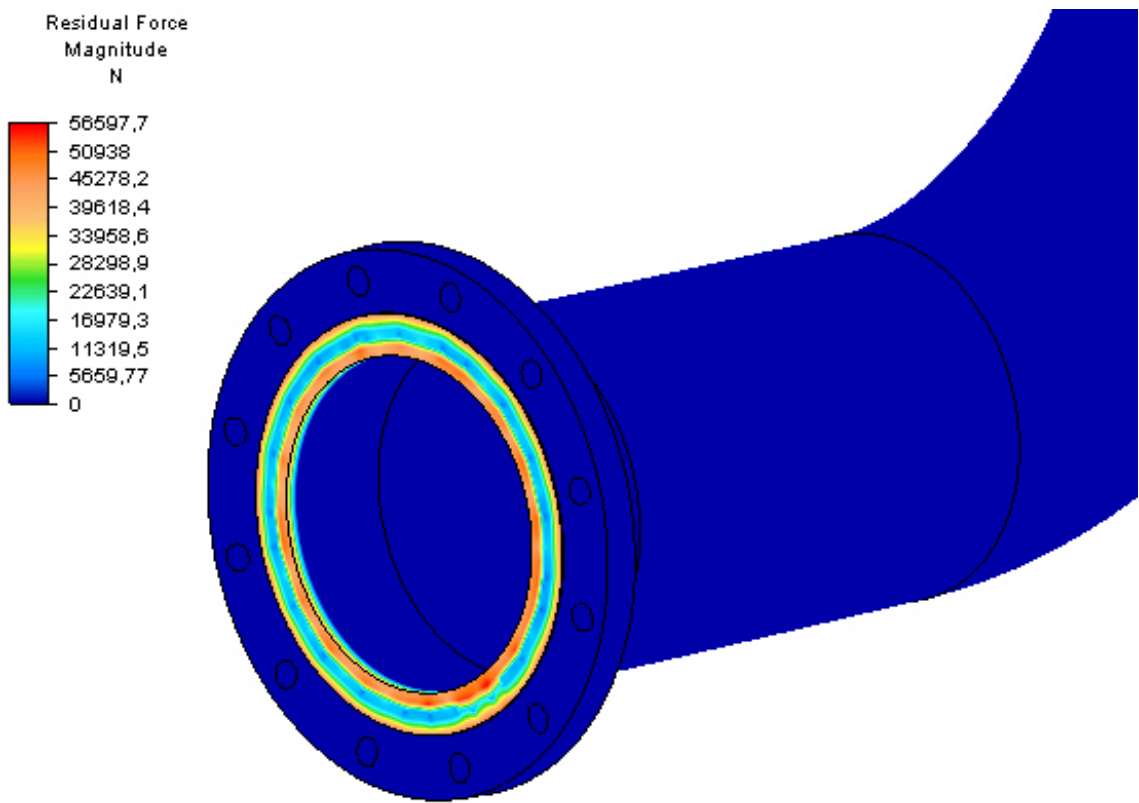


Figure 25: Magnitude of the reaction forces that are acting upon flange at the inlet.

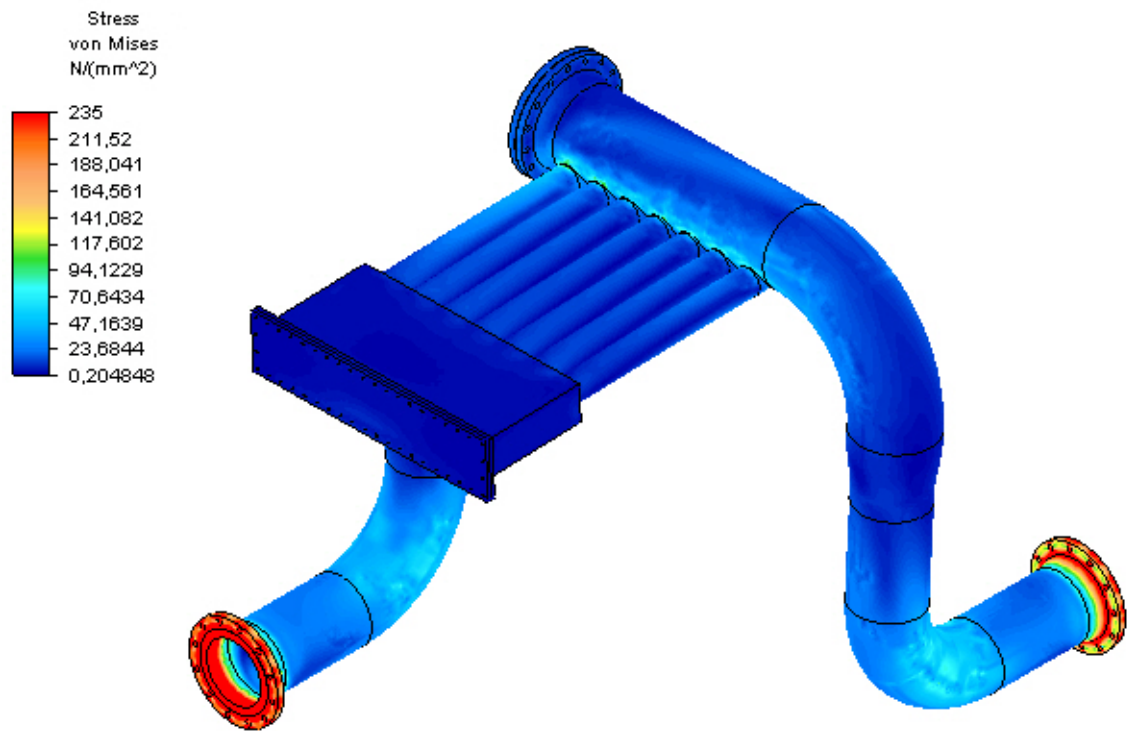


Figure 26: Von Mises stresses for the unit.

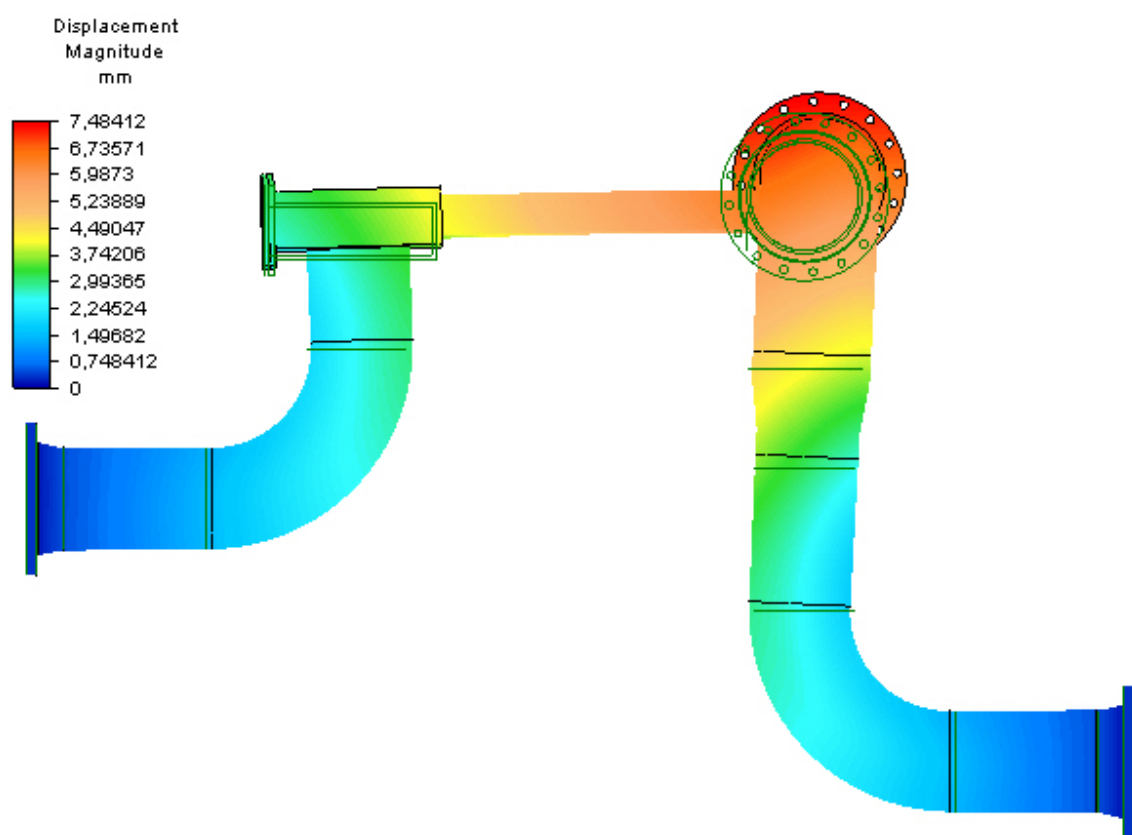


Figure 27: Displacement magnitude exaggerated by 2% of the model size

4.4 Uncertainty propagation results

In practice the working device does not often correlate to the calculated design due to dynamic variables that are not constant. To view how the thermal transfer is affected by various dynamic variables that were thought up as an example and how they affect the system as a whole. It is worth to note that the variables are assumed to be uncorrelated (independent) and random.

Table 10: Uncertainty propagation for thermal transfer in Scenario A

Dynamic variables	Variable \pm Uncert.	$\frac{\partial Q}{\partial X}$	% of uncert.
Effective external HTC (W/m ² -K)	55,59 \pm 5,559	804,4	94,0
Separator pressure (bar _a)	10 \pm 0,5	1778	3,7
Internal fouling factor (mm ² -K/W)	90 \pm 90	-7,6 x 10 ⁶	2,2
Face velocity (m/s)	4 \pm 0,2	492,8	0,1
External fouling factor (mm ² -K/W)	350 \pm 350	-0,16 x 10 ³	0,0
Ambient air pressure (bar _a)	0,95 \pm 0,0095	2062	0,0
Thermal transfer [W]	56.568 \pm 4611	-	-
Fan work [W]	1029 \pm 145	-	-
Steam quality [-]	99,836% \pm 0,015%	-	-

where the variable X in the partial derivative denotes the dynamic variable of interest.

As mentioned before the effective external heat transfer coefficient has a measurement uncertainty of $\pm 10\%$ and by taking that into account it is by far the most important factor in determining the thermal transfer rate.

Table 11: Uncertainty propagation for thermal transfer in Scenario B

Dynamic variables	Variable \pm Uncert.	$\frac{\partial Q}{\partial X}$	% of uncert.
Effective external HTC (W/m ² -K)	43,36 \pm 4,336	-32,1 x 10 ⁶	96,1
Separator pressure (bar _a)	10 \pm 0,5	-85,2 x 10 ⁶	2,4
Internal fouling factor (mm ² -K/W)	90 \pm 90	0,1838	1,4
Face velocity (m/s)	4 \pm 0,2	-27,8 x 10 ⁶	0,1
External fouling factor (mm ² -K/W)	350 \pm 350	-2,5 x 10 ⁻¹²	0,0
Ambient air pressure (bar _a)	0,95 \pm 0,0095	-73,1 x 10 ⁶	0,0
Thermal transfer [W]	54.809 \pm 4573	-	-
Fan work [W]	309,5 \pm 43	-	-
Steam quality [-]	99,841% \pm 0,015%	-	-

where the variable X in the partial derivative denotes the dynamic variable of interest.

All of the relative uncertainty selected for the variables are not directly based on any specific data, except for the effective external heat transfer coefficient which relies on uncertainty in measurements made by C. Weierman mentioned earlier.

Chapter 5

Conclusions

The device cleans the system by diluting the TDS concentration by approximately a factor of 10, for the presented scenarios, which might be of great benefit for turbine operators and to reduce the possibility of scaling. The downside is increased pressure loss to the turbine and a very small mass flow reduction, however these downsides are minimal compared to continuous operation of the turbine. Every hour that the turbine is off-line is a loss regarding electricity generation. Limits for normal continuous turbine operations can be seen on Table 1 showing the recommended TDS limits set by Mitsubishi and in Table 5 and 6 showing results from Scenario A and B. By assuming the quality of the separator and the demister the TDS concentration can vary, but determining the exact quality coming from either of those devices can be difficult due to the dynamic nature of the devices. Multiple measurements need to be taken regularly to get an idea on the performance of the devices, but numbers assumed in this paper are based generally on manufacturers data.

The low type fins on the pipe serve the best because the thermal conductivity of carbon steel is relatively low and by increasing the height of the fin the fin efficiency is reduced thus not utilizing the fins to their full potential. By maximizing the thermal transfer for the fins and minimizing the fan work required, taking into account the width of the unit, an optimized size was selected as the base scenario. The results showed a relatively good thermal heat transfer and minimal work required by the fan.

As is demonstrated on Figure 17 the serrated fins are performing better than the solid fins but they are very similar in thermal performance.

Fouling or scaling is often a common problem in the geothermal industry but usually the problem occurs in the two-phase side before the separator, in the brine outlet from the separator and during the low pressure stages in the turbine. When the steam has been

separated from the two-phase fluid the scaling is minimal compared to the brine side. But scaling can happen in the turbine, commonly the first two stages as the pressure drops and the droplets evaporate the TDS concentration increases as the droplet gets smaller, and that can carry high costs in regards to maintenance and life time of the turbine. By reducing the TDS concentration in the water droplets that enters the turbine you can effectively reduce the likelihood of mineral precipitation in the first two stages in the turbine, therefore reducing maintenance and downtime of the turbine.

The CFD analysis was used to determine the pressure loss through the device by analysing different designs and using two very common turbulence models from which the results show very similar pressure drop in most cases, we can to some degree of certainty deduct that the average pressure loss would be $0,11 \text{ bar}_a$ for a steady state operation.

As the CFD results indicate for Design 2 there is high velocity steam at the top pipe on Figure 23 to reduce the velocity we can either revert to Design 3 as is depicted in Appendix C on Figure 19 which results in more even velocity distribution. Design 4 is also an option however the front header is an impractical design and does not include a coverplate for the header. The option of adding another pipe to the tube banks provides a possibility to reduce the velocity but it increases the width and weight of the unit considerably and therefore the cost.

The reaction forces model was used to evaluate the thermal expansion of the device at steady state where the device was fixed at both ends. Resultant forces were approximately 29 kN at both ends when the device is fixed at both ends and undergoes thermal expansion. However it is worth to note that normally this is not how these types of devices are anchored, they would be on sliders or possibly, if the thermal expansion is large, have a expansion loop.

The uncertainty propagation can give an idea on how things might change or how accurate they might be, since the approach is an empirical relation we must assume some error in our calculations, according to C. Weierman the fit was in the $\pm 10\%$ range and we can assume our heat transfer is $56,6 \pm 4,6 \text{ kW}$ with the work being $1023 \pm 145 \text{ W}$ for scenario A and $54,8 \pm 4,6 \text{ kW}$ and the work being $318 \pm 44 \text{ W}$ in scenario B. That is assuming our internal heat transfer correlation is accurate, since we are border lining the two-phase region there is some uncertainty. The model assumes single phase internal heat transfer but certainly there is two-phase but since our steam is essentially dry steam we can make the assumption that there is no significant changes in the flow, NCG affect the heat transfer significantly as well and while in the two phase region we can see reduction in the internal heat transfer coefficient in the presence of NCG. Since our system is rather dynamic due to outside temperature changes and variable speed on the fan we have some

flexibility when it comes to dealing with the NCG and the determination of the internal heat transfer coefficient is less significant than the external heat transfer coefficient. The two-phase heat transfer coefficient (Shah) is significantly higher than the single phase heat transfer coefficient (Gnielinski) thus by assuming our true heat transfer coefficient lies somewhere in that range and with the presence of NCG we assume the lowest value which in return forces us to move more heat i.e. the fan needs to do more work.

As demonstrated by this model for Scenario A the quality of the steam initially is determined to be 99,99% and the exiting quality including the pressure drop is 99,836% \pm 0,015% for the serrated fins and 99,841% \pm 0,015% for the solid fins, this lower quality of steam results in more condensate formation resulting in diluted TDS, assuming all TDS is entrapped in the liquid.

To conclude the possibility of diluting the TDS in the condensate has been presented is a very viable option and will be further developed by Green Energy Group AS where they plan on building the device for their power plants.

References

- [1] IAPWS, “Formulation for the thermodynamic properties of ordinary water substance for general and scientific use,” 1995.
- [2] F-Chart Software, “Engineering Equation Solver,” calculations.
- [3] P. Valdimarsson, “Geothermal power plant cycles and main components,” *Proceedings of the short course on geothermal drilling, resource development and power plants. UNU-GTP and LaGeo, Santa Tecla, El Salvador*, pp. 1–24, January 2011.
- [4] R. DiPippo, *Geothermal Power Plants: Principles, Applications, Case Studies and Environmental Impact*, 2nd ed. Elsevier Science & Technology, November 2007, ch. 5, pp. 82–83.
- [5] A. Robin. (2012, December) Modes of heat transfer – conduction, convection & radiation. [Online]. Available: <http://www.spectrose.com/modes-of-heat-transfer-conduction-convection-radiation.html>
- [6] *TEMA Standards*, 8th ed., Tubular Exchanger Manufacturers Association, New York, 1999.
- [7] R. W. Serth and T. G. Lestina, *Process heat transfer: principles, applications and rules of thumb*, 2nd ed. Academic Press, February 2014, ch. 12, pp. 509–510.
- [8] Ekströms Värmetekniska AB. (2014) Helical fin tube, solid or serrated fins. [Online]. Available: <http://www.ekstromsvarme.se/helicalfintube.html>
- [9] Autodesk Knowledge Network. (2014, March) Mesh enhancement. [Online]. Available: <http://knowledge.autodesk.com/search?search=mesh%20enhancement>
- [10] Green Energy Group AS. (2014) Our solution. Green Energy Group AS. [Online]. Available: <http://www.geg.no/oursolution/>
- [11] V. V. der Mast, E. Goldman, and R. Soo-Hoo, “Steam Purity for Geothermal Power Plants,” *Geothermal Resources Council*, vol. 10, September 1986.

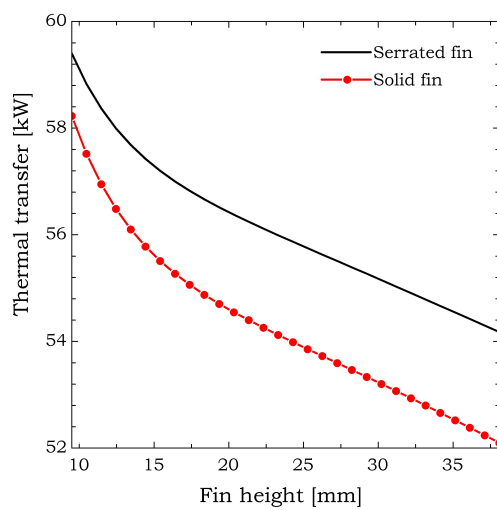
- [12] C. Ballzus, Þorbjörn Karlsson, and R. Maack, “Design of Geothermal Steam Supply Systems in Iceland,” *Geothermics*, vol. 21, no. 5/6, pp. 835–845, 1992.
- [13] V. Harðardóttir, “Metal-rich Scales in the Reykjanes Geothermal System, SW Iceland: Sulfide Minerals in a Seawater-dominated Hydrothermal Environment,” Ph.D. dissertation, University of Ottawa, 2011.
- [14] G. Axelsson and B. Steingrímsson, “Logging, testing and monitoring geothermal wells,” Short course on Geothermal Development and Geothermal Wells, March 2012, UNU-GTP.
- [15] Þráinn Friðriksson, A. A. Óladóttir, P. Jónsson, and E. I. Eyjólfsdóttir, “The Response of the Reykjanes Geothermal System to 100 MWe Power Production: Fluid Chemistry and Surface Activity,” in *Proceedings World Geothermal Congress 2010*. Bali, Indonesia: Iceland GeoSurvey, April 2010.
- [16] *Mitsubishi Turbine Operational Manual*, Mitsubishi.
- [17] S. J. Zarrouk and M. H. Purnanto, “Geothermal steam-water separators: Design overview,” in *Conference Paper Database*, International Geothermal Association, Ed. New Zealand Geothermal Workshop, November 2013.
- [18] K. Foong, “Design Concept for a More Efficient Steam-Water Separator,” in *World Geothermal Congress*. Antalya, Turkey: World Geothermal Congress, April 2005.
- [19] R. James, “Lectures on Geothermal Engineering,” UNU Geothermal training programme and Orkustofnun, Report 13, 1986.
- [20] F. P. Incropera, T. L. Bergman, A. S. Lavine, and D. P. DeWitt, *Fundamentals of Heat and Mass Transfer*, 7th ed. John Wiley and Sons, 2011, pp. 3–9.
- [21] A. D. Kraus, A. Aziz, and J. Welty, *Extended surface heat transfer*. John Wiley & Sons, 2001, ch. 1, p. 7.
- [22] S. Thorhallsson, “Common problems face in geothermal generation and how to deal with them,” *UNU-GTP*, January 2011, short Course on Geothermal Drilling, Resource Development and Power Plants.
- [23] Spiro-Gills, *Engineering Manual*, ESCOA Fintube Corporation, 1979.
- [24] V. Gnielinski, “New equations for heat and mass-transfer in turbulent pipe and channel flow,” *International Chemical Engineering*, vol. 16, no. 2, pp. 359–368, 1976.
- [25] F. P. Incropera, T. L. Bergman, A. S. Lavine, and D. P. DeWitt, *Fundamentals of Heat and Mass Transfer*, 7th ed. John Wiley and Sons, 2011, p. 545.

- [26] M. Shah, “A general correlation for heat transfer during film condensation inside pipes,” *International Journal of Heat and Mass Transfer*, vol. 22, no. 4, pp. 547–556, 1979.
- [27] M. M. Shah, “An improved and extended general correlation for heat transfer during condensation in plain tubes,” *HVAC&R Research*, vol. 15, no. 5, pp. 889–913, 2009.
- [28] F. P. Incropera, T. L. Bergman, A. S. Lavine, and D. P. DeWitt, *Fundamentals of Heat and Mass Transfer*, 7th ed. John Wiley and Sons, 2011, p. 522.
- [29] C. Weierman, “Correlations ease the selection of finned tubes,” *The Oil and Gas Journal*, no. 74, pp. 94–100, 1976.
- [30] R. W. Serth and T. Lestina, *Process heat transfer: principles, applications and rules of thumb*, 2nd ed. Academic Press, 2014, ch. 12, pp. 517–519.
- [31] B. E. Launder and D. B. Spalding, “The numerical computation of turbulent flows,” *Computer methods in applied mechanics and engineering*, vol. 3, no. 2, pp. 269–289, 1974.
- [32] H. K. Versteeg and W. Malalasekera, *An introduction to computational fluid dynamics: the finite volume method*. Pearson Education, 2007.
- [33] F. R. Menter, “Two-equation eddy-viscosity turbulence models for engineering applications,” *AIAA journal*, vol. 32, no. 8, pp. 1598–1605, 1994.
- [34] D. Wilcox, “Re-assessment of the scale-determining equation for advanced turbulence models,” *AIAA*, vol. 26, no. 11, pp. 1299–1310, 1988.
- [35] NASA Langley Research Center. (2013, August) The Menter Shear Stress Transport Turbulence Model. NASA. [Online]. Available: <http://turbmodels.larc.nasa.gov/sst.html>
- [36] B. N. Taylor and C. E. Kuyatt, “NIST Technical Note 1297,” *Guidelines for evaluating and expressing the uncertainty of NIST measurement results*, p. 24, 1994.
- [37] R. H. Perry and D. W. Green, *Perry’s Chemical Engineers Handbook*, 8th ed. McGraw-Hill, 2008, ch. 11, pp. 50–52.
- [38] API, “Air-Cooled Heat Exchangers for General Refinery Service,” American Petroleum Institute, Washington, D.C., DC, United States of America, API 661, March 2002.

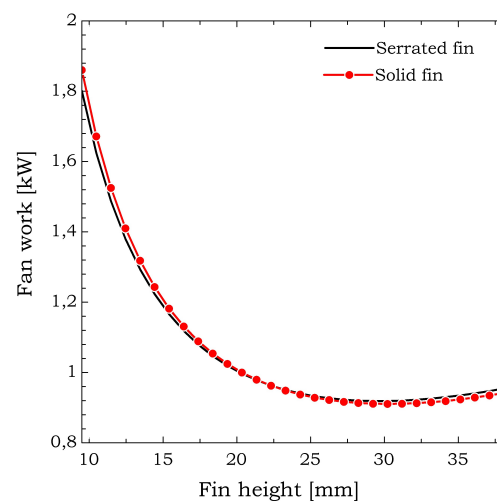
- [39] O. Jayaratne and B. Mason, “The coalescence and bouncing of water drops at an air/water interface,” *Proceedings of the Royal Society of London. Series A. Mathematical and Physical Sciences*, vol. 280, no. 1383, pp. 545–565, 1964.

Appendix A

Scenario A

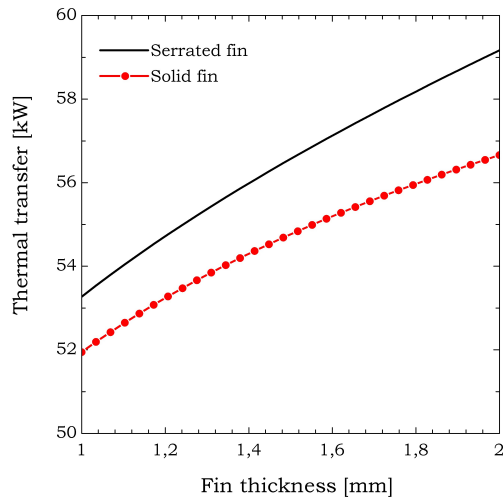


Thermal transfer as a function of fin height

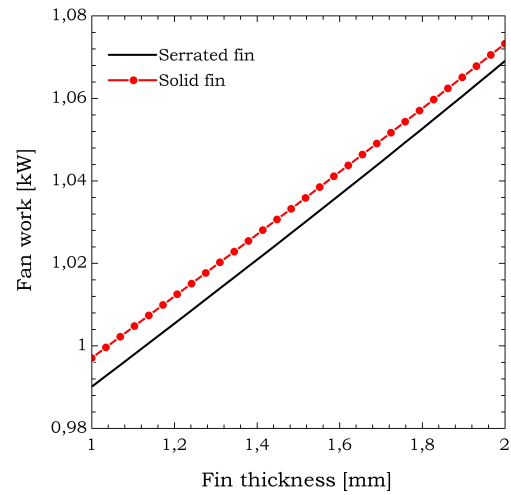


Fan work as a function of fin height

Figure 28: Thermal transfer for serrated and solid fins as a function of fin height

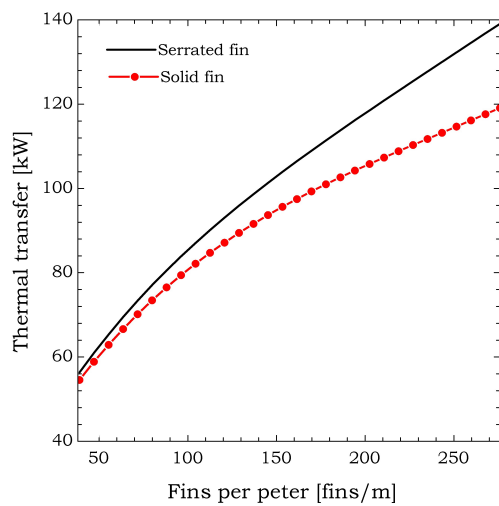


Thermal transfer as a function of fin thickness

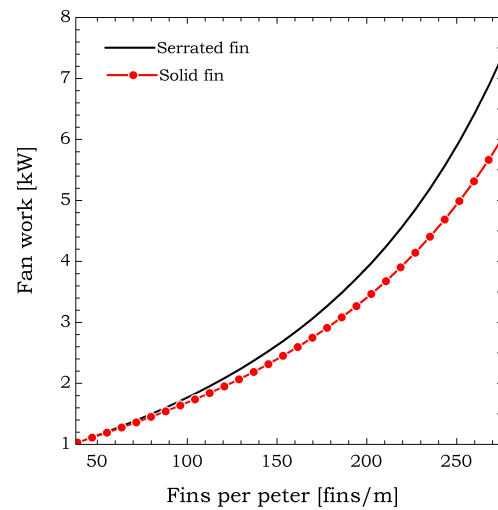


Fan work as a function of fin thickness

Figure 29: Thermal transfer for serrated and solid fins as a function of fin thickness

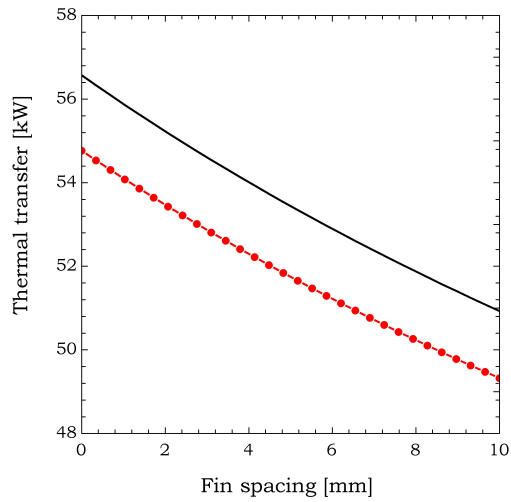


Thermal transfer as a function of fins per meter

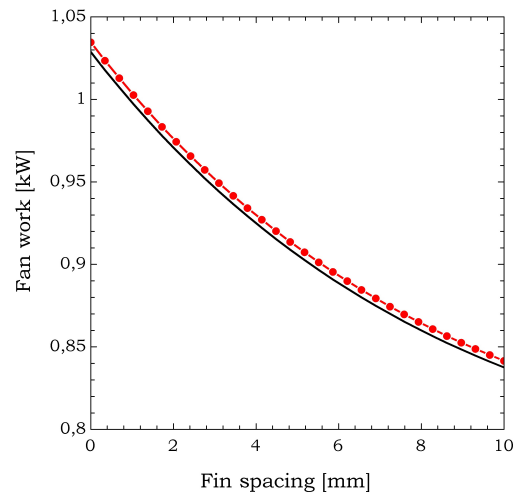


Fan work as a function of fins per meter

Figure 30: Thermal transfer for serrated and solid fins as a function of fins per meter

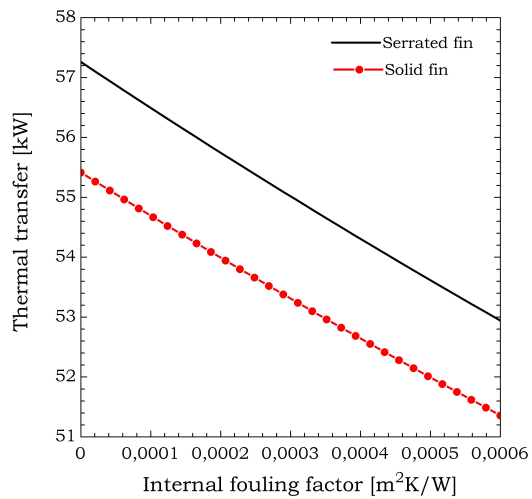


Thermal transfer as a function of fin spacing

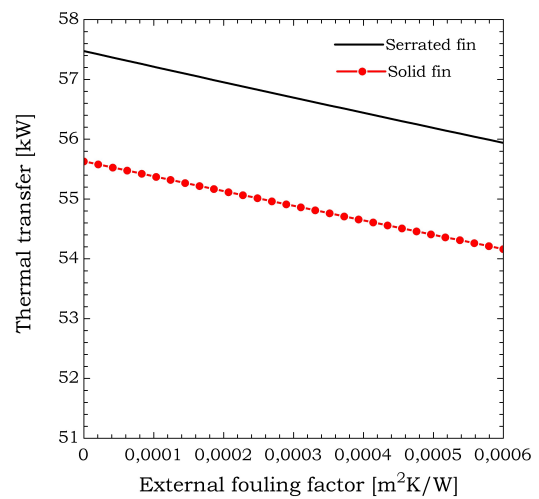


Fan work as a function of fin spacing

Figure 31: Thermal transfer for serrated and solid fins as a function of fin spacing



Thermal transfer as a function of the internal fouling factor

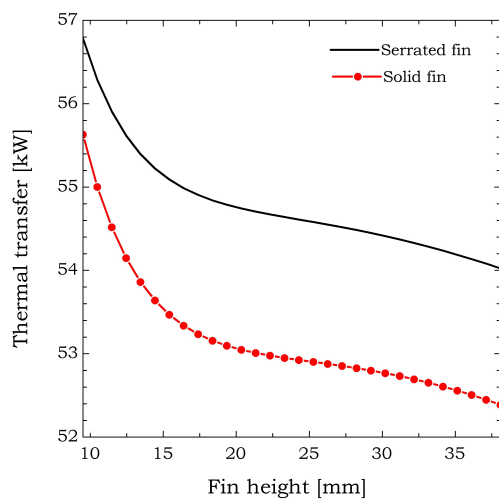


Thermal transfer as a function of the external fouling factor

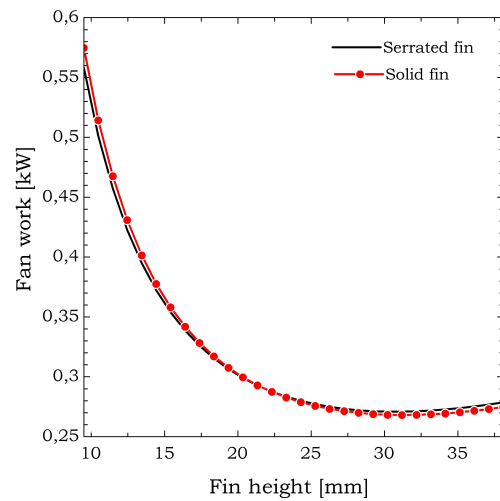
Figure 32: Thermal transfer for serrated and solid fins as a function of fouling factors

Appendix B

Scenario B

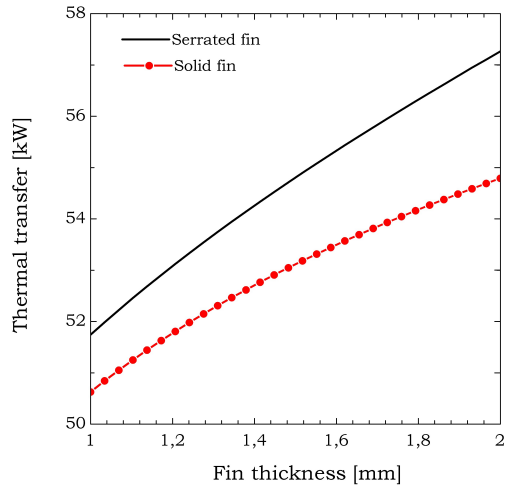


Thermal transfer as a function of fin height

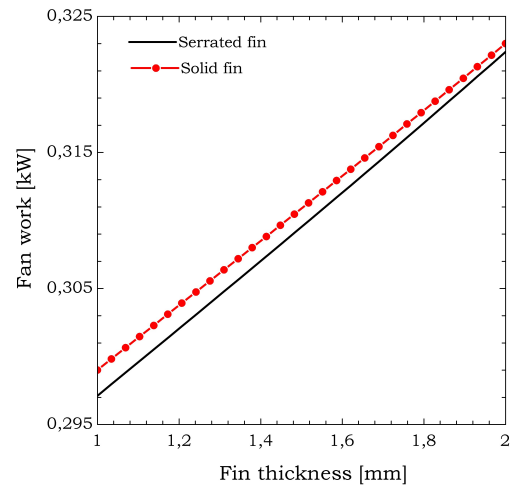


Fan work as a function of fin height

Figure 33: Thermal transfer for serrated and solid fins as a function of fin height

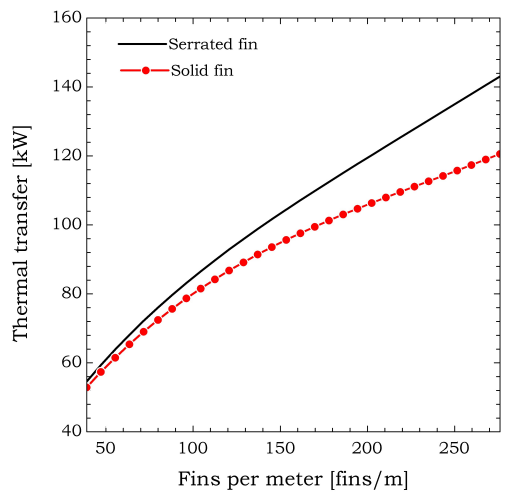


Thermal transfer as a function of fin thickness

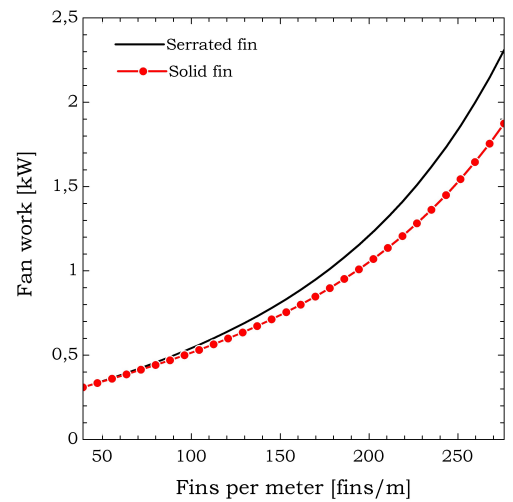


Fan work as a function of fin thickness

Figure 34: Thermal transfer for serrated and solid fins as a function of fin thickness

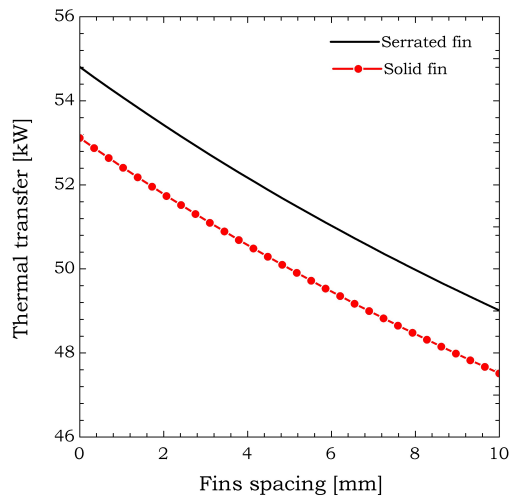


Thermal transfer as a function of fins per meter

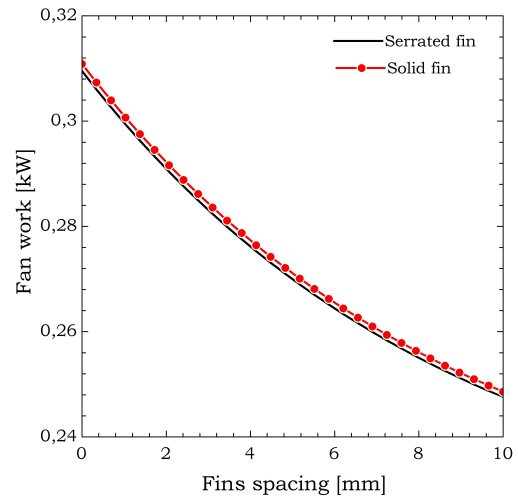


Fan work as a function of fins per meter

Figure 35: Thermal transfer for serrated and solid fins as a function of fins per meter

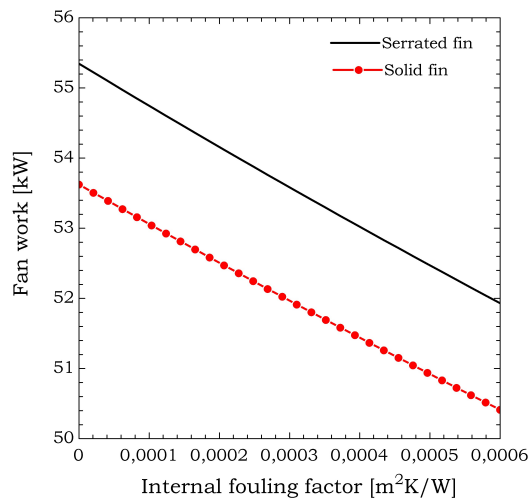


Thermal transfer as a function of fin spacing

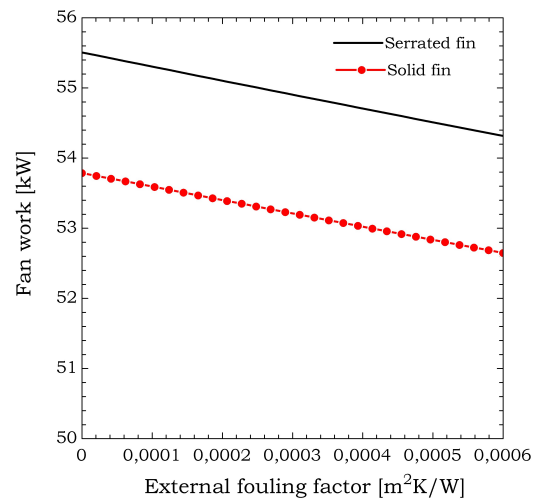


Fan work as a function of fin spacing

Figure 36: Thermal transfer for serrated and solid fins as a function of fin spacing



Thermal transfer as a function of the internal fouling factor



Thermal transfer as a function of the external fouling factor

Figure 37: Thermal transfer for serrated and solid fins as a function of fouling factors

Appendix C

Other designs

C.0.1 Design 1

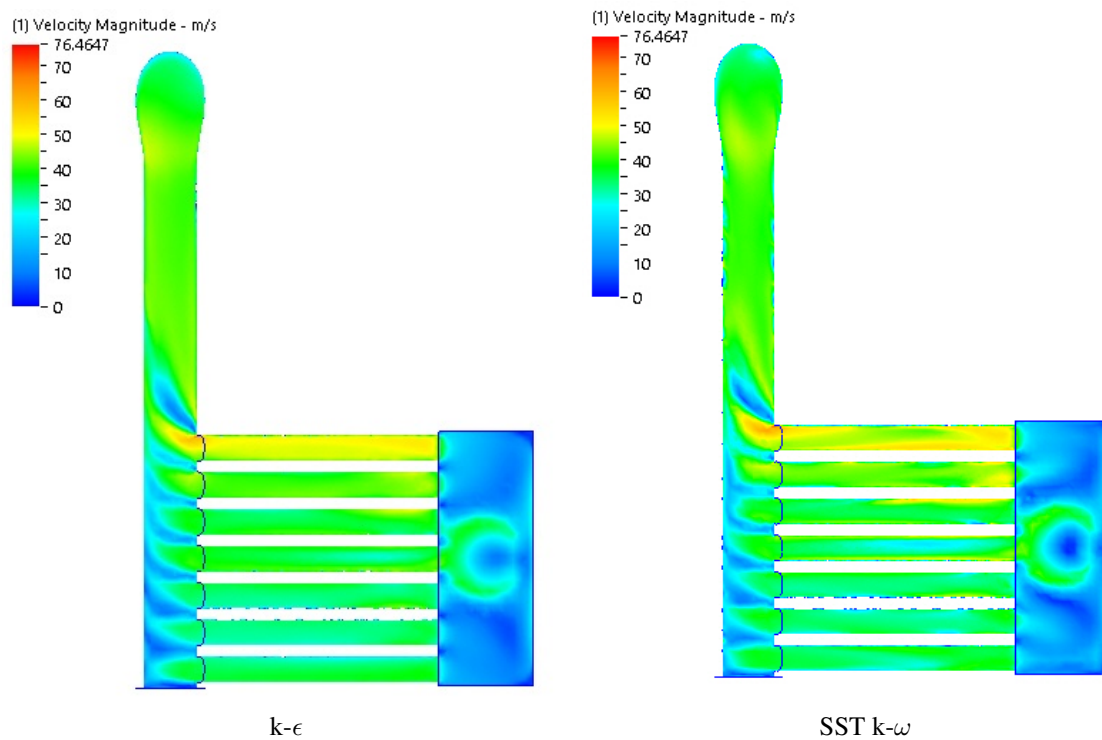
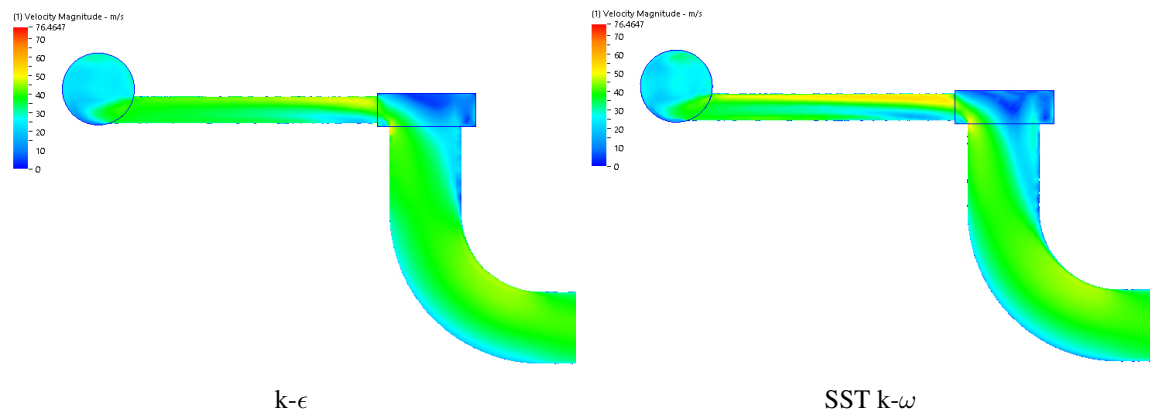
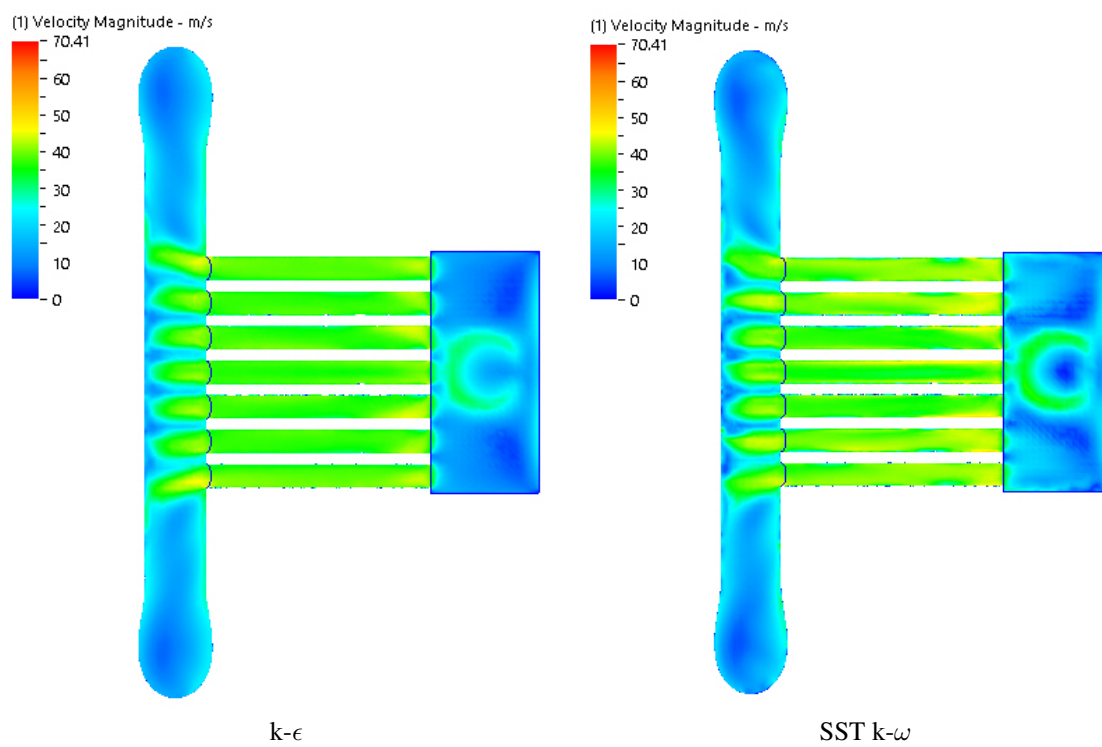
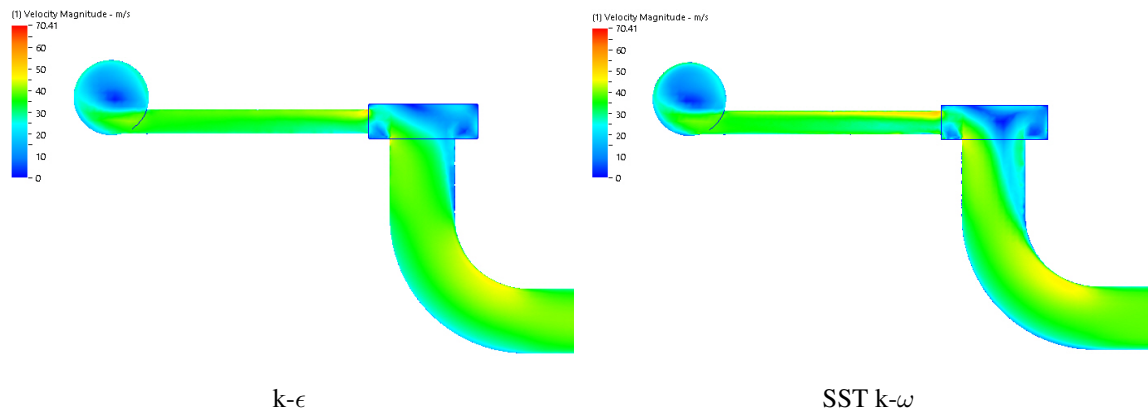


Figure 38: Topview of $k-\epsilon$ and SST $k-\omega$ on Design 1

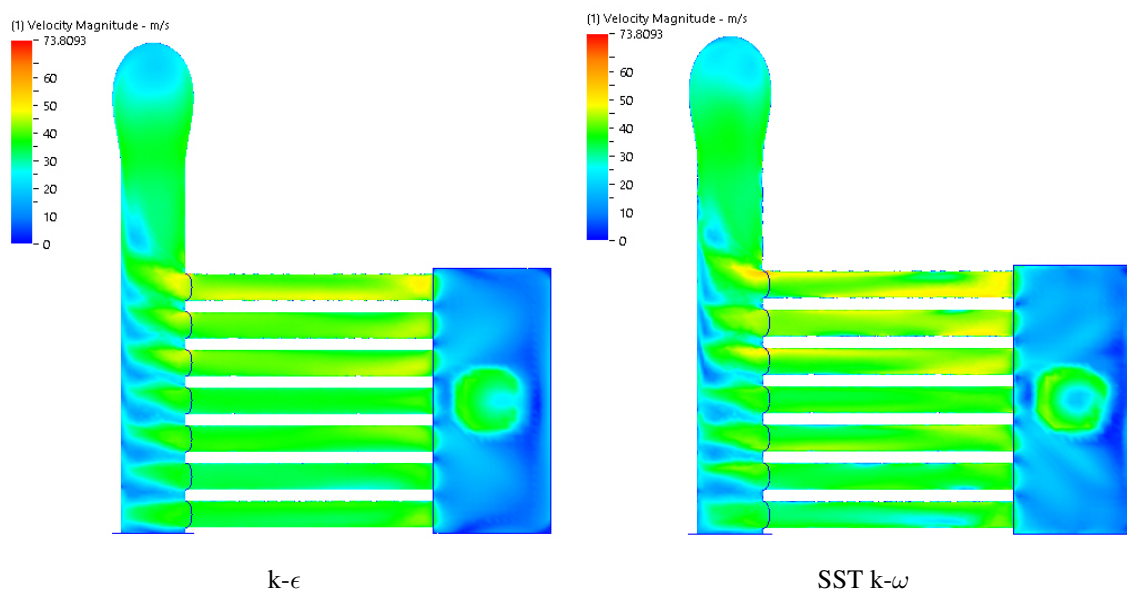
Figure 39: Sideview of k- ϵ and SST k- ω on Design 1

C.0.2 Design 3

Figure 40: Topview of k- ϵ and SST k- ω on Design 3

Figure 41: Sideview of $k-\epsilon$ and SST $k-\omega$ on Design 3

C.0.3 Design 4

Figure 42: Topview of $k-\epsilon$ and SST $k-\omega$ on Design 4

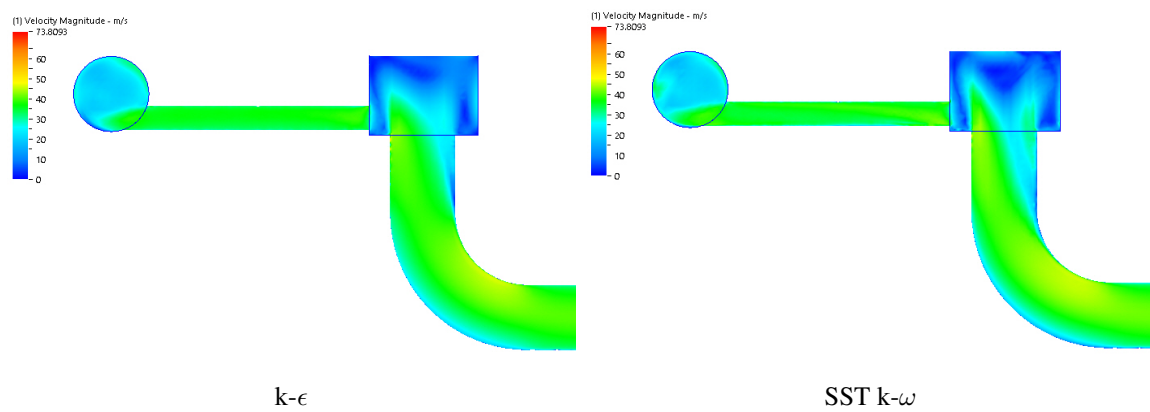


Figure 43: Sideview of $k-\epsilon$ and SST $k-\omega$ on Design 4



School of Science and Engineering
Reykjavík University
Menntavegi 1
101 Reykjavík, Iceland
Tel. +354 599 6200
Fax +354 599 6201
www.reykjavikuniversity.is
ISSN 1670-8539